
Coarse-Grained Boltzmann Generators

Weilong Chen^{*1} Bojun Zhao^{*1} Jan Eckwert¹ Julija Zavadlav^{1,2}

Abstract

Sampling equilibrium molecular configurations from the Boltzmann distribution is a longstanding challenge. Boltzmann Generators (BGs) address this by combining exact-likelihood generative models with importance sampling, but practical scalability is limited. Meanwhile, coarse-grained surrogates enable the modeling of larger systems by reducing effective dimensionality, yet often lack a reweighting procedure required to ensure asymptotically correct statistics. In this work, we propose Coarse-Grained Boltzmann Generators (CG-BGs), a framework for reduced-order generative modeling with importance sampling in coarse-grained coordinate space. CG-BGs generate samples using a flow-based model and reweight them using a learned potential of mean force (PMF). We show that the PMF can be learned from rapidly converged trajectories via enhanced sampling force matching. Experiments demonstrate that CG-BGs capture solvent-mediated interactions in highly reduced representations while substantially reducing computational cost relative to atomistic BGs, providing a practical route toward equilibrium sampling of larger molecular systems.

1. Introduction

Accurately sampling molecular configurations from the Boltzmann distribution is a central problem in statistical physics (Chandler, 1987). These samples are required for estimating observables and thermodynamic quantities, including free energies (Chipot & Pohorille, 2007). For molecular systems, the high dimensionality of the configuration

space makes direct computation of the partition function intractable, forcing a reliance on simulation methods such as Molecular Dynamics (MD) or Markov Chain Monte Carlo (MCMC) (Frenkel & Smit, 2002). However, these methods are often inefficient in systems with rugged energy landscapes. High free energy barriers lead to metastable trapping, producing strongly correlated samples and slow convergence (Lindorff-Larsen et al., 2011). Despite extensive progress in enhanced sampling methods (Zhu et al., 2025; Hénin et al., 2022) (e.g., umbrella sampling (Torrie & Valleau, 1977), metadynamics (Laio & Gervasio, 2008)) and coarse-graining (Noid, 2013; Saunders & Voth, 2013), equilibrium sampling at scale remains difficult.

Deep generative models have recently emerged as a promising alternative for equilibrium sampling (Noé et al., 2019; Albergo et al., 2019; Wirnsberger et al., 2020). A notable example is the Boltzmann Generator (BG) (Noé et al., 2019). By learning a diffeomorphic transformation between a simple prior (e.g., a Gaussian) and the complex molecular configuration space, BGs enable efficient proposal generation and exact-likelihood evaluation. The tractable likelihood permits rigorous reweighting of generated configurations to the target Boltzmann distribution via importance sampling, allowing unbiased estimation of equilibrium observables. This has enabled amortized sampling strategies (Tan et al., 2025b), where generation is substantially cheaper than MD simulations.

In practice, however, scaling BGs to high-dimensional molecular systems remains difficult (Klein & Noé, 2024; Tan et al., 2025a). As system size increases, even expressive generative models exhibit diminishing overlap with the target distribution, resulting in high-variance importance weights and ineffective reweighting. In addition, likelihood evaluation requires Jacobian determinant computation (Chen et al., 2018), which introduces significant computational overhead and scales poorly with dimensionality (Hutchinson, 1989). As a result, existing BG applications are largely restricted to small systems such as short peptides (Tan et al., 2025b; Rehman et al., 2025) with empirical implicit solvent models (Hawkins et al., 1995; Nguyen et al., 2013).

Coarse-graining (CG) provides a complementary approach by projecting atomistic configurations onto a lower-dimensional set of collective variables. This idea underlies

^{*}Equal contribution, random order. ¹Professorship of Multi-scale Modeling of Fluid Materials, Department of Engineering Physics and Computation, TUM School of Engineering and Design, Technical University of Munich, Germany ²Atomistic Modeling Center, Munich Data Science Institute, Technical University of Munich, Germany. Correspondence to: Julija Zavadlav <julija.zavadlav@tum.de>.

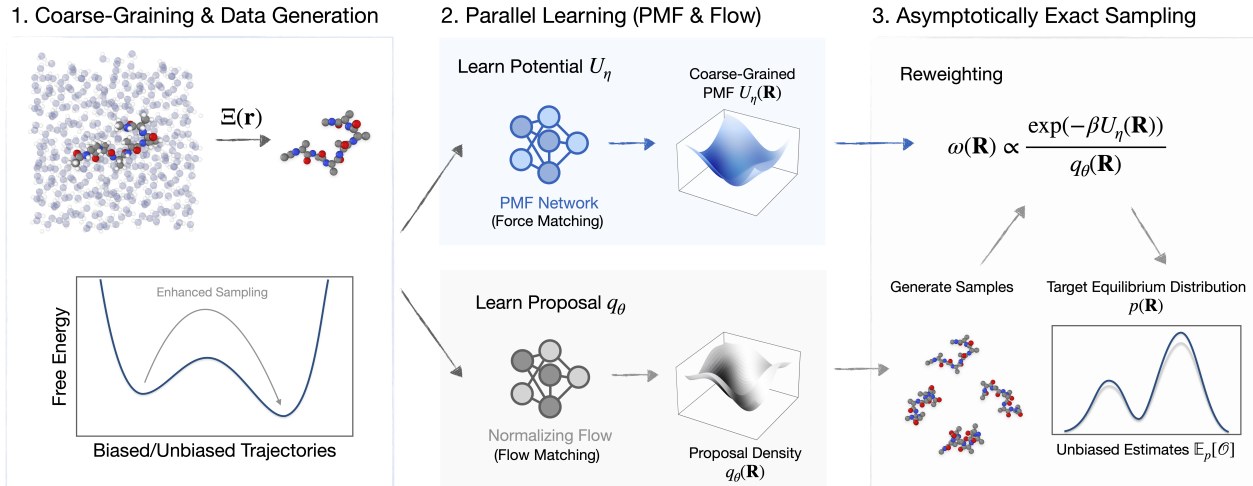


Figure 1. CG-BG framework. Atomistic configurations are mapped to CG coordinates to construct training data. A PMF network learns $U_\eta(\mathbf{R})$ from rapidly converged data, while a normalizing flow learns a proposal density $q_\theta(\mathbf{R})$ over CG configurations. Samples generated from the flow are reweighted using the PMF to recover the target equilibrium distribution $p(\mathbf{R})$, enabling unbiased estimation of thermodynamic observables.

Boltzmann Emulators (Lewis et al., 2025; Zheng et al., 2024; Jing et al., 2024; Zhu et al., 2026) and related generative surrogates (Schreiner et al., 2023; Daigavane et al., 2025; Plainer et al., 2025; Costa et al., 2025; dos Santos Costa et al., 2024; Diez et al., 2025; Vlachas et al., 2021; Xu et al., 2025). By reducing the number of degrees of freedom during generation, these methods can be applied to larger systems. However, training requires converged unbiased simulation data, which is difficult to obtain in practice. Thus, CG models are often trained on short finite-time trajectories that do not fully capture the target distribution (Lewis et al., 2025; Zheng et al., 2024) and, unlike Boltzmann Generators, do not incorporate reweighting to correct this mismatch due to the lack of an explicit energy function for the target distribution, resulting in biased statistical estimates.

Present work. In this paper, we introduce *Coarse-Grained Boltzmann Generators* (CG-BGs, Fig. 1), a class of Boltzmann Generators that operate directly in CG coordinates¹. CG-BGs combine generative modeling with importance sampling using a learned potential of mean force (PMF) as the target energy, enabling asymptotically correct equilibrium sampling in a reduced-dimensional representation. This design provides a scalable pathway for sampling high-dimensional molecular systems. CG-BGs are particularly advantageous as they can be trained directly from rapidly converged data and effectively capture complex solvent-mediated effects.

Our main contributions are:

¹Our code is publicly available at <https://github.com/tummmf/cg-bg>.

- We introduce *Coarse-Grained Boltzmann Generators*, a scalable framework for equilibrium sampling in CG coordinate space using **machine learning potentials** (MLPs) as the target energy for importance sampling.
- We show that enhanced sampling force matching enables learning the PMF from rapidly converged simulation trajectories, eliminating reliance on unbiased equilibrium data and providing a correction mechanism for Boltzmann Emulators.
- We demonstrate that CG-BGs capture solvent-mediated interactions in highly reduced representations, achieving improved accuracy over classical implicit solvent models while substantially reducing computational cost relative to atomistic BGs.

2. Background and Preliminaries

Notation. We use lowercase variables for fine-grained (atomistic) quantities and uppercase variables for CG quantities.

We consider a many-body system with configuration $\mathbf{r} \in \mathbb{R}^n$ governed by a potential energy function $u(\mathbf{r})$. At thermodynamic equilibrium with temperature T , the system follows the Boltzmann distribution

$$p(\mathbf{r}) = \frac{e^{-\beta u(\mathbf{r})}}{Z}, \quad Z = \int e^{-\beta u(\mathbf{r})} d\mathbf{r}, \quad (1)$$

where $\beta = (k_B T)^{-1}$ and Z is the partition function. The goal of equilibrium sampling is to generate samples from $p(\mathbf{r})$ in order to compute observables $\mathbb{E}_p[\mathcal{O}] =$

$\int \mathcal{O}(\mathbf{r})p(\mathbf{r})d\mathbf{r}$, and free energies. A dataset is considered converged if empirical averages of observables match their equilibrium expectations within statistical error.

2.1. Boltzmann Generators and Emulators

Boltzmann Generators (BGs) (Noé et al., 2019) combine exact-likelihood generative models with importance sampling to estimate equilibrium properties. Typically implemented using normalizing flows (Rezende & Mohamed, 2016), a BG defines a tractable proposal density $q_\theta(\mathbf{r})$ that approximates $p(\mathbf{r})$. Given samples $\mathbf{r}_i \sim q_\theta$, importance weights are computed as

$$w(\mathbf{r}_i) = \frac{p(\mathbf{r}_i)}{q_\theta(\mathbf{r}_i)} \propto \frac{e^{-\beta u(\mathbf{r}_i)}}{q_\theta(\mathbf{r}_i)}. \quad (2)$$

Unbiased estimates of equilibrium expectations are then obtained using the self-normalized importance sampling estimator

$$\mathbb{E}_p[\mathcal{O}] \approx \frac{\sum_{i=1}^N w(\mathbf{r}_i) \mathcal{O}(\mathbf{r}_i)}{\sum_{i=1}^N w(\mathbf{r}_i)}. \quad (3)$$

Provided that q_θ overlaps sufficiently with p , this estimator converges to the corresponding Boltzmann averages. This allows BGs to be trained on biased or non-equilibrium samples, with reweighting correcting the induced distribution shift at evaluation.

Boltzmann Emulators adopt similar generative architectures but omit the reweighting step, relying directly on q_θ for estimating observables. Model accuracy is therefore determined by the quality of the learned distribution q_θ , with no correction applied at inference time. This places stronger requirements on the training data: accurate models require long unbiased trajectories, which are difficult to obtain in practice.

2.2. Continuous Normalizing Flows

Continuous normalizing flows (CNFs) extend discrete normalizing flows (Dinh et al., 2014; Rezende & Mohamed, 2016) by modeling density transformations as solutions to time-dependent ordinary differential equations (ODEs) (Chen et al., 2018). A vector field $v_\theta : [0, 1] \times \mathbb{R}^n \rightarrow \mathbb{R}^n$, parameterized by a neural network, defines the dynamics

$$\frac{d\mathbf{x}(t)}{dt} = v_\theta(t, \mathbf{x}(t)), \quad \mathbf{x}(0) \sim p_0, \quad (4)$$

where p_0 is a simple prior distribution. The solution at time t is

$$\mathbf{x}(t) = \mathbf{x}(0) + \int_0^t v_\theta(\tau, \mathbf{x}(\tau)) d\tau. \quad (5)$$

The evolution of the log-density follows the instantaneous change-of-variables formula

$$\log p_t(\mathbf{x}(t)) = \log p_0(\mathbf{x}(0)) - \int_0^t \nabla \cdot v_\theta(\tau, \mathbf{x}(\tau)) d\tau, \quad (6)$$

where $\nabla \cdot v_\theta$ denotes the divergence of the vector field.

While CNFs are often trained using maximum likelihood, Flow Matching (FM) (Lipman et al., 2022; Liu et al., 2022; Albergo et al., 2023) provides a simulation-free alternative. Conditional Flow Matching (CFM) (Tong et al., 2023) directly regresses the neural vector field v_θ onto a target conditional vector field $u_t(\mathbf{x} | z)$ that induces a prescribed probability path. The training objective is

$$\mathcal{L}_{\text{CFM}}(\theta) = \mathbb{E}_{t,z,\mathbf{x} \sim p_t(\cdot|z)} [\|v_\theta(t, \mathbf{x}) - u_t(\mathbf{x} | z)\|^2], \quad (7)$$

where $t \sim \mathcal{U}[0, 1]$ and z is a conditioning variable. A common choice uses linear interpolation between paired source and target samples (Albergo et al., 2023; Tong et al., 2023). Let $z = (\mathbf{x}_0, \mathbf{x}_1)$ with \mathbf{x}_0 and \mathbf{x}_1 sampled from the source and target distributions, respectively. The interpolated state and corresponding vector field are

$$\mathbf{x}_t = (1-t)\mathbf{x}_0 + t\mathbf{x}_1, \quad u_t(\mathbf{x}_t | \mathbf{x}_0, \mathbf{x}_1) = \mathbf{x}_1 - \mathbf{x}_0. \quad (8)$$

2.3. Coarse-Graining and Potentials of Mean Force

Coarse-graining maps atomistic configurations $\mathbf{r} \in \mathbb{R}^n$ to a lower-dimensional set of collective variables (CVs), or *beads*, $\mathbf{R} \in \mathbb{R}^N$ with $N \ll n$, through a mapping $\mathbf{R} = \Xi(\mathbf{r})$. The CG variables are typically chosen to retain the slow degrees of freedom. In *bottom-up* coarse-graining (Noid et al., 2008; Jin et al., 2022), the objective is to construct an effective CG potential such that the CG model reproduces the marginal equilibrium distribution of the atomistic system:

$$p(\mathbf{R}) = \int p(\mathbf{r}) \delta(\Xi(\mathbf{r}) - \mathbf{R}) d\mathbf{r}. \quad (9)$$

This marginal distribution admits a Boltzmann form,

$$p(\mathbf{R}) \propto e^{-\beta U(\mathbf{R})}, \quad (10)$$

where the effective energy $U(\mathbf{R})$, known as the *potential of mean force*, is defined up to an additive constant as

$$U(\mathbf{R}) = -k_B T \ln \int e^{-\beta u(\mathbf{r})} \delta(\Xi(\mathbf{r}) - \mathbf{R}) d\mathbf{r}. \quad (11)$$

The PMF includes both energetic and entropic contributions from the eliminated degrees of freedom and generally contains many-body, state-dependent interactions (Krishna et al., 2009).

Evaluating the PMF is intractable in practice due to the high-dimensional integral over \mathbf{r} . Classical CG force fields (Marink et al., 2007; Souza et al., 2021) approximate $U(\mathbf{R})$ using fixed functional forms, which may lack sufficient expressivity. More recent approaches represent $U(\mathbf{R})$ using neural networks trained by force matching (Noid et al., 2008; Wang et al., 2019) or relative entropy minimization (Shell, 2008; Thaler et al., 2022).

3. Coarse-Grained Boltzmann Generators

Atomistic BGs permit reweighting-based equilibrium sampling but become difficult to apply to large systems. Boltzmann Emulators improve scalability by omitting reweighting, at the cost of introducing bias.

We introduce CG-BGs, which perform generative modeling and importance sampling directly in CG coordinate space. Instead of the full atomistic distribution, CG-BGs target the marginal distribution $p(\mathbf{R})$ defined by the PMF.

CG-BGs consist of two components: a flow-based model that generates CG configurations and a learned PMF used for importance reweighting. Unlike atomistic MLPs trained on labeled energies (Blank et al., 1995; Behler & Parrinello, 2007), CG PMFs cannot be directly evaluated from atomistic configurations because they include entropic contributions from eliminated degrees of freedom. We next describe how the PMF is learned from atomistic simulations and outline the CG-BG workflow (Fig. 1).

3.1. Variational Force Matching

Variational Force Matching (VFM) (Noid et al., 2008), also known as multiscale coarse-graining, is a bottom-up approach for learning the PMF from atomistic forces.

The central condition is that CG forces should match, in expectation, the instantaneous atomistic forces projected onto the CG coordinates, denoted by $\mathcal{F}_{\text{proj}}(\mathbf{r})$. The exact PMF satisfies:

$$-\nabla U(\mathbf{R}) = \mathbb{E}_{p(\mathbf{r}|\mathbf{R})} [\mathcal{F}_{\text{proj}}(\mathbf{r})]. \quad (12)$$

where the expectation is taken over the *fiber distribution* (Hummerich et al., 2025), i.e., the conditional distribution of atomistic configuration \mathbf{r} given \mathbf{R} .

From a learning perspective, instantaneous projected forces provide stochastic estimates of the conditional mean force in Eq. (12). Given a dataset \mathcal{D} of atomistic configurations, a parameterized CG potential $U_\eta(\mathbf{R})$ is trained by minimizing

$$\mathcal{L}_{\text{VFM}}(\eta) = \mathbb{E}_{\mathbf{r} \sim \mathcal{D}} \left[\left\| \nabla_{\mathbf{R}} U_\eta(\Xi(\mathbf{r})) + \mathcal{F}_{\text{proj}}(\mathbf{r}) \right\|_2^2 \right]. \quad (13)$$

When \mathcal{D} is sampled from equilibrium, this objective minimizes the Fisher divergence between the model distribution $p_\eta(\mathbf{R})$ and the true marginal $p(\mathbf{R})$. Theoretical error bounds follow from Log-Sobolev inequalities (Proof in §A.1):

Proposition 1. *Let $p^*(\mathbf{R}) \propto e^{-\beta U^*(\mathbf{R})}$ be the true marginal and $p_\eta(\mathbf{R}) \propto e^{-\beta U_\eta(\mathbf{R})}$ the learned distribution. If p^* satisfies a Logarithmic Sobolev Inequality (LSI) with constant $\rho > 0$. Then, the Kullback-Leibler divergence between the learned and true distributions*

is bounded by the expected squared force error:

$$\mathcal{D}_{\text{KL}}(p_\eta \| p^*) \leq \frac{\beta^2}{2\rho} \mathbb{E}_{p_\eta} \left[\left\| \nabla U_\eta(\mathbf{R}) - \nabla U^*(\mathbf{R}) \right\|^2 \right]. \quad (14)$$

While global LSI conditions are strong assumptions for multimodal PMFs (Vempala & Wibisono, 2019), this result motivates force matching as a proxy for distributional accuracy. This is relevant for importance sampling, where performance depends on the divergence between the learned and true marginal distributions.

3.2. Enhanced Sampling for Force Matching

Standard force matching requires unbiased converged data, which is expensive to obtain for systems with metastable states and large free energy barriers—a limitation shared by Boltzmann Emulators. In addition, high-energy transition regions are rarely visited under the Boltzmann distribution, yet are important for accurately learning the PMF.

Enhanced sampling force matching (ESFM) (Chen et al., 2026) overcomes these limitations by using invariance of the fiber distribution under coarse-grained biasing.

Proposition 2. (Chen et al. (2026)) *Let $V(\mathbf{R})$ be a bias potential depending only on the coarse-grained coordinates. The conditional distribution of atomistic configurations given \mathbf{R} is invariant:*

$$p_V(\mathbf{r} | \mathbf{R}) = p(\mathbf{r} | \mathbf{R}). \quad (15)$$

Since the mean force $-\nabla U(\mathbf{R})$ is an expectation of the projected forces over this conditional distribution (Eq. 12), the regression target is unchanged under CG biasing. ESFM minimizes

$$\mathcal{L}_{\text{ESFM}}(\eta) = \mathbb{E}_{\mathbf{r} \sim \mathcal{D}_{\text{bias}}} \left[\left\| \nabla_{\mathbf{R}} U_\eta(\Xi(\mathbf{r})) + \mathcal{F}_{\text{proj}}(\mathbf{r}) \right\|_2^2 \right], \quad (16)$$

where $\mathcal{D}_{\text{bias}}$ is a rapidly converged dataset generated using enhanced sampling and $\mathcal{F}_{\text{proj}}(\mathbf{r})$ denotes forces recomputed from the unbiased atomistic potential.

Proposition 3. (Chen et al. (2026)) *Minimizing $\mathcal{L}_{\text{ESFM}}$ yields the same global optimum as standard force matching loss \mathcal{L}_{VFM} , assuming sufficient model expressivity.*

Together, Propositions 2 (Proof in §A.2) and 3 establish that ESFM enables accurate PMF learning from biased enhanced sampling data, benefiting from faster convergence and improved coverage of transition regions.

3.3. The CG-BG Workflow

After training, the learned PMF U_η defines the target energy for importance sampling, rather than as a force field for MD

integration. Let $q_\theta(\mathbf{R})$ denote the density induced by the trained flow model. Importance weights are computed as

$$w(\mathbf{R}) \propto \frac{\exp(-\beta U_\eta(\mathbf{R}))}{q_\theta(\mathbf{R})}. \quad (17)$$

Provided U_η accurately approximates the true PMF on the support of q_θ , reweighting gives unbiased estimates under $p(\mathbf{R})$ in the idealized setting where the PMF is exact. In practice, the learned PMF introduces approximation bias.

The reliability of importance reweighting is quantified by the normalized effective sample size (ESS) (Kish, 1965),

$$\text{ESS} = \frac{1}{B} \frac{\left(\sum_{i=1}^B w(\mathbf{R}_i)\right)^2}{\sum_{i=1}^B w(\mathbf{R}_i)^2}. \quad (18)$$

where B denotes the number of generated samples. The normalized ESS takes values in $(0, 1]$, with larger values indicating better overlap between the generative density q_θ and the target density defined by U_η . In practice, machine learning potentials may exhibit unphysical extrapolation outside the training domain, and generative models may occasionally produce high-energy artifacts, both of which can lead to weight degeneracy. To improve robustness, we apply a weight clipping strategy (Tan et al., 2025a; Gloy & Olsson, 2025; Moqvist et al., 2025) to truncate statistical outliers before computing expectations (See §G.4). The complete CG-BG training and sampling pipeline is summarized in Fig. 1.

4. Experiments

We evaluate CG-BGs on the Müller–Brown (MB) potential and three alanine peptide systems, including alanine dipeptide (Ac-Ala-NHMe, 22 atoms), alanine tripeptide (Ac-Ala₃-NHMe, 42 atoms), and alanine hexapeptide (Ac-Ala₆-NHMe, 72 atoms). Additional experimental details including architectures are provided in §C and §D. CG-BG samples are generated and reweighted following the algorithms described in §F.

Datasets. For all systems, we construct unbiased and biased datasets for training and evaluation. Biased datasets are generated using enhanced sampling methods to accelerate exploration. For the MB system, data are generated via Langevin dynamics (§B.1), with umbrella sampling (Torrie & Valleau, 1977) used in the biased setting to improve transitions between metastable basins. For peptide systems, datasets are generated using both explicit and implicit solvent models (§B.2). Explicit solvent data are produced using a classical force field (Lindorff-Larsen et al., 2010) and include long unbiased MD trajectories as well as biased simulations obtained via well-tempered metadynamics (Barducci et al., 2008). Implicit solvent data are generated using the same force field in combination with a generalized

Born model under different parameterizations (OBC1 and OBC2) (Onufriev et al., 2004). For explicit solvent simulations, configurations are further coarse-grained using either a *Heavy Atom* mapping (Fig. 2a and Fig. 4a), which retains all heavy atoms, or a *Core Beta* mapping (Fig. 2f and Fig. 4f), which retains backbone atoms and the C_β position. Full details on dataset generation and enhanced sampling procedures are provided in §B.

Baselines. Unlike previous BG work (Klein & Noé, 2024; Tan et al., 2025a;b), which often treats implicit solvent simulations as reference, we use explicit solvent simulations as the primary reference and treat empirical implicit solvent models as baselines. We additionally report results from atomistic BGs, including TarFlow and ECNF++ (Tan et al., 2025b) trained on implicit solvent simulation data.

Metrics. We report ESS, Jensen-Shannon (JS) divergence, and PMF error. JS divergence is computed between the sampled and reference dihedral angle free energy profiles. The PMF error is defined as the squared distance between the negative logarithms of the sampled and reference densities, placing additional emphasis on low-probability regions compared to JS divergence (Plainer et al., 2025; Durumeric et al., 2024). Energy histograms and free energy profiles of ϕ dihedral are shown in the main text, while additional results, including ψ dihedral free energy profiles, Ramachandran plots (Ramachandran, 1963), bond length distributions, and weight clipping ablations, are provided in §G.

4.1. Recovering Equilibrium Distributions from Biased and Unbiased Data

We first demonstrate that CG-BGs inherit the importance reweighting capability of atomistic BGs, enabling recovery of equilibrium statistics from flow models trained on either biased or unbiased trajectories.

For the MB system (Fig. 6), coarse-graining corresponds to projection onto the x -coordinate, yielding an analytically exact reference $U(x) = -k_B T \ln \int \exp(-\beta u(x, y)) dy$ (Fig. 6c–d). For peptides, we use two CG mappings depending on system size: the Heavy Atom mapping for alanine dipeptide and tripeptide (Fig. 2a and Fig. 4a), and the Core Beta mapping for hexapeptide (Fig. 4f). Throughout §4.1 and §4.2, the PMF is learned from rapidly converged datasets using ESFM (§3.2).

As shown in Fig. 2c, Fig. 4c, 4h and Fig. 6c, despite training on long unbiased datasets and using expressive models, the raw flow proposals deviate from the MD reference. These discrepancies arise from low-quality samples generated by the flow model, a limitation intrinsic to Boltzmann Emulators that cannot be systematically corrected without reweighting. After reweighting, CG-BGs successfully recover equilibrium free energy profiles in close agreement

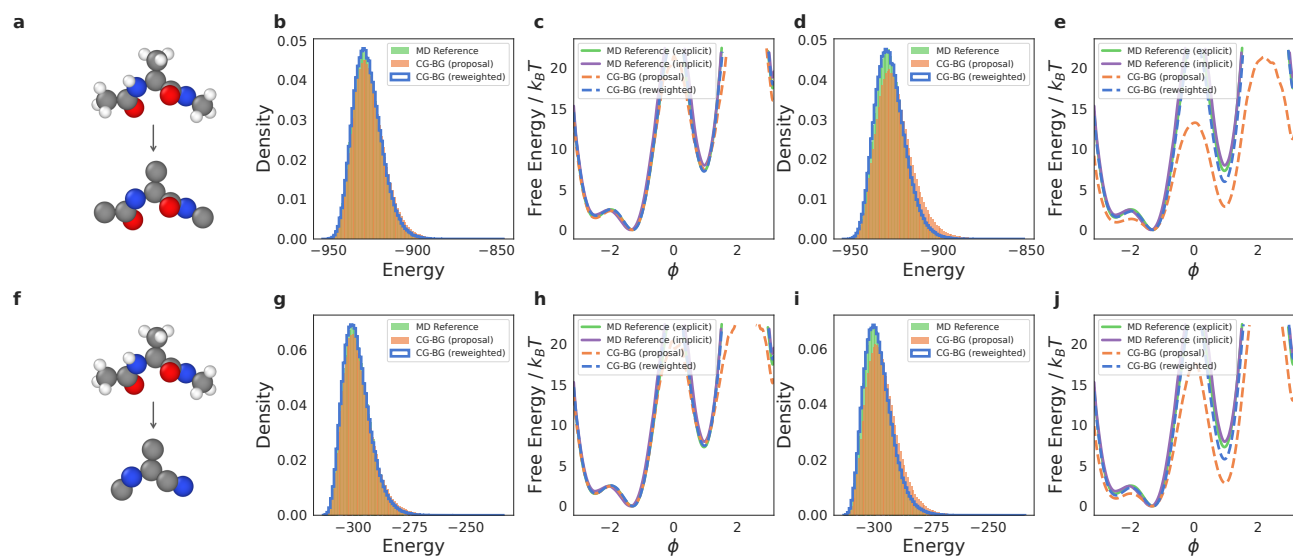


Figure 2. CG-BGs on alanine dipeptide. (a–e) Heavy Atom mapping results. (a) Heavy Atom mapping. (b) Potential energy distribution under the learned PMF for flow trained on 500 ns *unbiased* data, before and after reweighting, compared with MD reference. (c) ϕ dihedral free energy profile for the same model. (d) Energy distribution for flow trained on 10 ns *WT-MetaD* ($\gamma = 1.5$) data. (e) Corresponding ϕ dihedral free energy profile. (f–j) Core Beta mapping results are shown in the second row with the same structure as (a–e).

with MD references. The reweighted distributions accurately reproduce relative basin populations and match the reference distribution in transition regions. This is further illustrated by the Ramachandran plots (Fig. 3, Fig. 4e and Fig. 4j). Unweighted proposals exhibit noisy samples across transition areas and metastable basins (Fig. 8 and Fig. 9), which are assigned low importance weights and effectively filtered out after reweighting. Quantitative metrics in Tab. 2 confirm close agreement between reweighted samples and target equilibrium ensemble.

We further evaluate CG-BGs trained on biased or short non-equilibrium trajectories (umbrella sampling for MB and 10 ns *WT-MetaD* with $\gamma = 1.5$ for alanine dipeptide), reflecting realistic settings where long unbiased simulations are infeasible. As shown in Fig. 2 and Fig. 6f, while the flow proposals exhibit larger deviations from the MD reference, importance reweighting consistently recovers accurate equilibrium statistics (Tab. 2).

Notably, after reweighting, CG-BGs outperform implicit solvent MD baselines (Tab. 2), highlighting the advantage of learning PMFs from explicit solvent simulations. While implicit solvent models perform reasonably well for alanine dipeptide, we observe increasing differences for tripeptide (Fig. 4c) and hexapeptide (Fig. 4h), consistent with previous observations for more complex molecular systems (Chen et al., 2021). This constitutes an improvement over atomistic BG approaches, which rely on implicit solvent models for reweighting and are therefore fundamentally limited by solvent approximation error. In other words, atomistic BGs can at best achieve the accuracy of implicit solvent baselines (Tab. 2 and Tab. 7). These results show that CG-BGs generate CG equilibrium samples consistent with the target distribution, without requiring long unbiased MD simulations, and offer a practical route to correct systematic biases in existing Boltzmann Emulators.

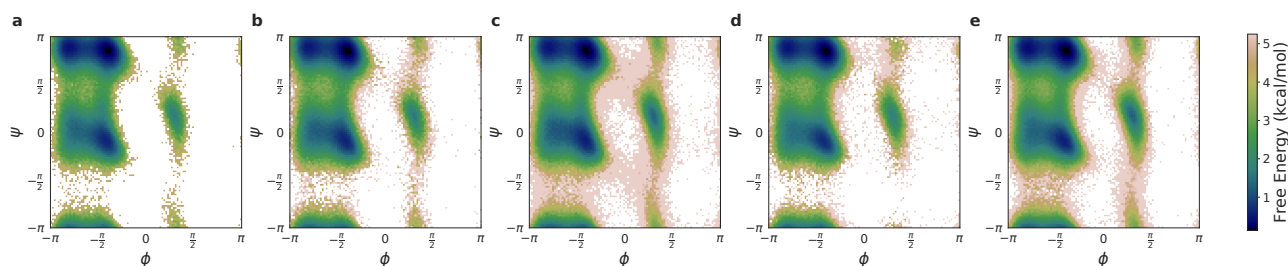


Figure 3. Ramachandran plots of alanine dipeptide. (a) MD reference. (b,c) Heavy Atom mapping: reweighted Ramachandran distributions. In (b), the flow model is trained on 500 ns *unbiased* data; in (c), it is trained on 10 ns *WT-MetaD* ($\gamma = 1.5$) data. (d,e) Core Beta mapping: same training setups as (b,c). Unweighted Ramachandran plots are provided in Fig. 8.

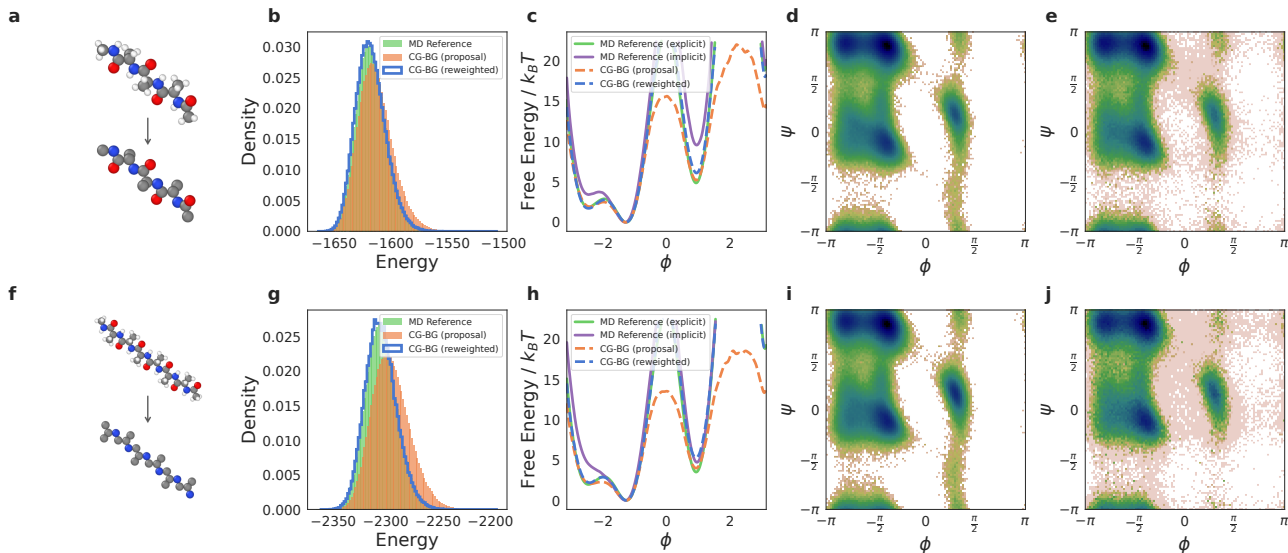


Figure 4. CG-BGs on alanine tripeptide and hexapeptide. (a–e) Alanine tripeptide (Heavy Atom mapping): (a) CG representation, (b) potential energy distribution, (c) ϕ free energy profile, (d) MD reference Ramachandran plot, and (e) reweighted Ramachandran distribution. (f–j) Alanine hexapeptide (Core Beta mapping): (f) CG representation, (g) potential energy distribution, (h) ϕ free energy profile, (i) MD reference Ramachandran plot, and (j) reweighted Ramachandran distribution. Unweighted Ramachandran plots are shown in Fig. 9. The reported free energy profiles and Ramachandran plots correspond to the dihedral pair biased during WT-MetaD: the second pair (of three) for alanine tripeptide and the third pair (of six) for alanine hexapeptide, counting from the N-methyl terminus.

4.2. Effect of Coarse-Graining Resolution on Accuracy and Efficiency

We next examine how the choice of CG resolution affects both sampling quality and computational efficiency. To this end, we consider a coarser Core Beta mapping for alanine dipeptide (Fig. 2f) and tripeptide (Fig. 7a). Despite the reduced resolution, CG-BGs trained with the Core Beta mapping remain capable of recovering equilibrium statistics after reweighting (Fig. 2h, 2j and Fig. 7c), with quantitative metrics reported in Tab. 2 and Tab. 3.

Compared to the Heavy Atom mapping, the lower-dimensional Core Beta representation generally yields higher ESS, indicating improved overlap between the flow proposal and the target distribution. This is expected, as generative modeling and importance sampling become easier in lower-dimensional spaces. Nevertheless, after reweighting, the resulting equilibrium statistics are generally less accu-

rate than those obtained with the Heavy Atom mapping. A likely explanation is the increased degeneracy introduced by coarse-graining. For a given CG coordinate \mathbf{R} , many atomistic microstates \mathbf{r}_i satisfy $\Xi(\mathbf{r}_i) = \mathbf{R}$ while exerting different projected forces $\mathcal{F}_{\text{proj}}(\mathbf{r}_i)$. As a result, the conditional mean force $\mathbb{E}_{p(\mathbf{r}|\mathbf{R})}[\mathcal{F}_{\text{proj}}(\mathbf{r})]$ exhibits larger variance under coarser mappings, increasing the difficulty of accurately learning the PMF through force matching. This effect is expected to become more pronounced as molecular complexity increases (Görlich & Zavadlav, 2025).

We further benchmark the computational cost of CG-BGs across different resolutions (Tab. 1). As expected, the Core Beta mapping substantially reduces both training and inference time compared to the Heavy Atom and full atomistic representations, with particularly large gains at inference due to cheaper Jacobian evaluations. Note that the reported all atom baseline generates only solute coordinates; generating full configurations with explicit solvent, which would be the proper reference, is computationally infeasible. Overall, the results illustrate a trade-off between statistical efficiency and representation fidelity: coarser mappings improve proposal quality and computational efficiency, while finer mappings show more accurate equilibrium estimates after reweighting. Additional comparisons with prior work are provided in Tab. 5.

Table 1. Training and inference time across different CG mappings on alanine dipeptide. Inference times correspond to 10^4 generated samples. *All Atom* denotes generating the full solute configuration without solvent.

Stage	Core Beta	Heavy Atom	All Atom
Training	0.45h	0.80h	2.55h
Inference	0.95min	3.78min	14.91min
Total	0.47h	0.86h	2.80h

4.3. Simulation-Free Evaluation of Learned PMFs

Beyond equilibrium sampling, CG-BGs provide a form of amortized equilibrium benchmarking for learned PMFs. Whereas conventional BGs use a learned proposal distribution to estimate observables under a fixed target energy, the same proposal distribution can also be reused to evaluate and compare multiple candidate PMFs through importance reweighting. Once a sufficiently accurate proposal has been learned, equilibrium observables under different PMFs can be estimated from a single set of generated samples, without performing additional simulations.

Specifically, the flow model generates CG configurations from a proposal distribution approximating the equilibrium ensemble, and importance reweighting maps these samples to the Boltzmann distribution induced by a given PMF. This enables rapid, simulation-free assessment of candidate CG potentials, in contrast to traditional validation pipelines that require separate MD simulations for each model.

We leverage this capability to compare PMFs trained under different data regimes, contrasting models learned from long unbiased MD trajectories (PMF_U) with those trained on a rapidly converged biased dataset (PMF_B). Quantitative metrics from reweighted samples (Tab. 2) provide a direct measure of model accuracy, while dihedral free energy profiles and Ramachandran plots enable visual comparison with atomistic references. Consistent with previous observations (Chen et al., 2026; Görlich & Zavadlav, 2025), PMF_U (Fig. 5) fails to recover the correct metastable populations along ϕ , whereas PMF_B exhibits improved agreement.

Although demonstrated here for CG models, the same principle naturally extends to atomistic machine learning potentials. More generally, generated configurations can be reused to compare multiple learned energy functions without additional simulations, making CG-BGs a practical tool for rapid model validation.

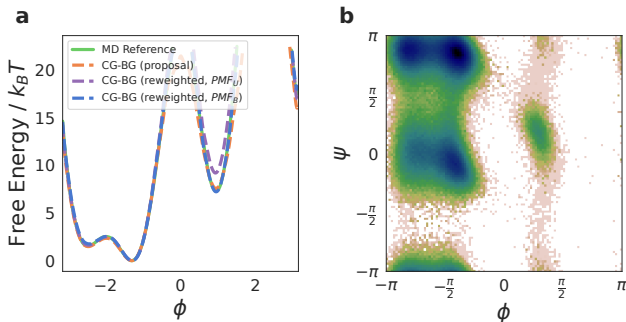


Figure 5. Simulation-free benchmarking of learned CG PMFs using CG-BGs on alanine dipeptide (Heavy Atom). (a) ϕ free energy profile after reweighting with PMFs trained on unbiased (PMF_U) and rapidly converged biased datasets (PMF_B), compared with the MD reference and flow proposal (trained on unbiased data). (b) Ramachandran plot reweighted using PMF_U .

Table 2. Quantitative comparison for alanine dipeptide across CG resolutions and baseline models. CG-BGs results are reported after reweighting; *Biased* denotes flow trained on WT-MetaD datasets, while PMF_U indicates PMFs learned from long unbiased MD data. Flow proposal results are provided in Tab. 7.

Model	JS (\downarrow)	PMF (\downarrow)	ESS (\uparrow)
CG-BGs (Reweighted)			
Heavy Atom	0.0048(1)	0.2005(63)	0.5112(4)
Heavy Atom (Biased)	0.0063(1)	0.2277(66)	0.4115(4)
Core Beta	0.0052(1)	0.2210(65)	0.5528(4)
Core Beta (Biased)	0.0057(1)	0.2093(58)	0.4818(4)
Heavy Atom (PMF_U)	0.0050(1)	0.2131(68)	0.5196(4)
Implicit Solvent Baselines			
GB (OBC1)	0.0157(2)	0.3709(92)	–
GB (OBC2)	0.0182(2)	0.4028(95)	–

5. Related Work

Generative models for equilibrium molecular sampling.

Generative models have emerged as powerful tools for sampling Boltzmann distributions (Olsson, 2026; Klein et al., 2023; Rotskoff, 2024; Aranganathan et al., 2025; Janson & Feig, 2025; Xie et al., 2026). Subsequent work has improved BGs in various ways (von Klitzing et al., 2025; Schebek & Rogal, 2025; OuYang et al., 2026), including the incorporation of inductive biases (Köhler et al., 2020), improved transferability across chemical and thermodynamic conditions (Klein & Noé, 2024; Dibak et al., 2022; Moqvist et al., 2025; Invernizzi et al., 2022), and more scalable architectures and likelihood estimators (Tan et al., 2025a; Zhai et al., 2024; Gloy & Olsson, 2025; Rehman et al., 2025; Peng & Gao, 2025). Several approaches address the resolution gap between coarse-grained and atomistic representations through backmapping (Chennakesavalu et al., 2023; Hummerich et al., 2025; Wang et al., 2022) or other reconstruction strategies (Schopmans & Friederich, 2024; Stupp & Koutsourelakis, 2025). Closely related to our setting, Tamagnone et al. (2024) combine a normalizing flow over collective variables with nonequilibrium dynamics to evolve the remaining degrees of freedom. Kohler et al. (2023) instead use a normalizing flow to model the coarse-grained distribution and generate configurations and forces for training coarse-grained MLPs via force matching. Another active line of research considers neural samplers for sampling unnormalized densities (Akhound-Sadegh et al., 2024; Midgley et al., 2023; He et al., 2025; Potapchik et al., 2025; Liu et al., 2025), which also have applications in molecular systems (Nam et al., 2025; Havens et al., 2025; Blessing et al., 2026).

Coarse-grained machine learning potentials. The development of CG MLPs can be viewed as an extension of

Table 3. Quantitative comparison for alanine tripeptide and hexapeptide across CG resolutions and baseline models. CG-BGs results are reported after reweighting. Flow proposal results are provided in Tab. 8 and Tab. 9.

Model	Alanine Tripeptide			Alanine Hexapeptide		
	JS (\downarrow)	PMF (\downarrow)	ESS (\uparrow)	JS (\downarrow)	PMF (\downarrow)	ESS (\uparrow)
Core Beta	0.0060(1)	0.2112(51)	0.4212(5)	0.0100(1)	0.3646(81)	0.1231(3)
Heavy Atom	0.0056(1)	0.1957(52)	0.3201(4)	—	—	—
Implicit Solvent Baselines						
GB (OBC2)	0.0932(3)	1.0274(65)	—	0.1652(3)	1.8401(70)	—

broader effort to construct accurate machine learning interatomic potentials from first-principles calculations. (Batzner et al., 2022; Batatia et al., 2022; Unke et al., 2021). Beyond *bottom-up* approaches (Jin et al., 2022; Noid, 2013), CG potentials can also be parameterized using *top-down* methods that reproduce macroscopic observables or experimental measurements (Marrink et al., 2007; Thaler & Zavadlav, 2021; Fuchs & Zavadlav, 2025). Recent work has explored different machine learning approaches for learning CG MLPs (Zhang et al., 2018; Wang et al., 2019; Kohler et al., 2023; Arts et al., 2023; Plainer et al., 2025). Despite these advances, learning transferable and computationally efficient CG MLPs remains challenging (Charron et al., 2025; Mirarchi et al., 2024; Majewski et al., 2023; Durumeric et al., 2023). A limitation of standard force matching objectives is their strong reliance on large amounts of converged simulation data. ESFM (Chen et al., 2026) addresses this by learning from rapidly converged biased simulations. Alternative strategies include constrained MD approaches for approximating mean forces prior to training (Ciccotti et al., 2005; Park et al., 2026; Fan et al., 2026).

6. Conclusion

This work introduces CG-BGs, a scalable framework for equilibrium sampling of coarse-grained molecular systems. By targeting the marginal equilibrium distribution defined by the PMF, CG-BGs reduce the effective dimensionality of the sampling problem while retaining asymptotic correctness through importance reweighting. The underlying PMF can be learned from rapidly converged data using enhanced sampling force matching, providing a correction mechanism for existing CG Boltzmann Emulators. Even at high levels of coarse-graining, CG-BGs capture solvent-mediated and many-body effects, and enable one-shot, simulation-free evaluation of CG MLPs.

Limitations. The current approach uses predefined collective variables for coarse-graining and enhanced sampling, which may be nontrivial to identify for complex systems. Recent advances in collective variable discovery (Zhang et al., 2024; Ribeiro et al., 2018; Chen & Ferguson, 2018;

Herringer et al., 2023; Mehdi et al., 2024) and uncertainty quantification (Zaverkin et al., 2024; Musil et al., 2019) provide promising avenues to address these challenges.

Future work. Extending CG-BGs to larger, more complex systems is a natural next step, leveraging demonstrated transferability of generative models (Didi et al., 2026; Antoniadis et al., 2026) and MLPs (Wood et al., 2025; Kabylda et al., 2025). More broadly, advances in exact-likelihood generative modeling, including autoregressive architectures (Rehman et al., 2026; Yu et al., 2026), as well as improvements in atomistic Boltzmann Generators, can be readily transferred to the CG setting. The simulation-free evaluation method introduced here also opens the possibility of elucidating the design space of coarse-grained machine learning potentials. It could enable systematic assessment of how architectural choices, parameterizations, and training objectives influence PMF accuracy. In contrast to conventional pipelines that rely on validation loss or repeated MD simulations, this approach could provide direct assessment of model quality via observable level comparisons. Finally, while CG-BGs are trained from simulation data in this work, one could also explore energy-based training or more general neural sampler formulations using the learned PMFs as unnormalized targets.

Acknowledgements

We thank Simon Olsson, Franz Görlich, Nuno Costa, and Paul Fuchs for fruitful discussions and helpful feedback. This work was funded by the European Union through the ERC (StG SupraModel) - 101077842. Views and opinions expressed are however those of the author(s) only and do not necessarily reflect those of the European Union or the European Research Council Executive Agency. Neither the European Union nor the granting authority can be held responsible for them.

Impact Statement

This work focuses on sampling from Boltzmann distributions, a problem of broad interest in machine learning and

AI for Science, with applications in both statistical physics and molecular simulations. We introduce Coarse-Grained Boltzmann Generators, which can be trained on molecular systems and applied to tasks such as drug and material discovery. While we do not anticipate immediate negative impacts, we encourage careful consideration when scaling these methods to prevent potential misuse.

References

- Abramson, J., Adler, J., Dunger, J., Evans, R., Green, T., Pritzel, A., Ronneberger, O., Willmore, L., Ballard, A. J., Bambrick, J., et al. Accurate structure prediction of biomolecular interactions with alphafold 3. *Nature*, pp. 1–3, 2024.
- Akhound-Sadegh, T., Rector-Brooks, J., Bose, A. J., Mittal, S., Lemos, P., Liu, C.-H., Sendera, M., Ravanbakhsh, S., Gidel, G., Bengio, Y., et al. Iterated denoising energy matching for sampling from boltzmann densities. *arXiv preprint arXiv:2402.06121*, 2024.
- Albergo, M. S., Kanwar, G., and Shanahan, P. E. Flow-based generative models for markov chain monte carlo in lattice field theory. *Physical Review D*, 100(3):034515, 2019.
- Albergo, M. S., Boffi, N. M., and Vanden-Eijnden, E. Stochastic interpolants: A unifying framework for flows and diffusions. *arXiv preprint arXiv:2303.08797*, 2023.
- Antoniadis, P., Pavesi, B., Olsson, S., and Winther, O. Protein language model embeddings improve generalization of implicit transfer operators. *arXiv preprint arXiv:2602.11216*, 2026.
- Aranganathan, A., Gu, X., Wang, D., Vani, B. P., and Tiwary, P. Modeling boltzmann-weighted structural ensembles of proteins using artificial intelligence-based methods. *Current opinion in structural biology*, 91:103000, 2025.
- Arts, M., Garcia Satorras, V., Huang, C.-W., Zügner, D., Federici, M., Clementi, C., Noé, F., Pinsler, R., and van den Berg, R. Two for One: Diffusion Models and Force Fields for Coarse-Grained Molecular Dynamics. *Journal of Chemical Theory and Computation*, 19(18): 6151–6159, September 2023. ISSN 1549-9618. doi: 10.1021/acs.jctc.3c00702.
- Barducci, A., Bussi, G., and Parrinello, M. Well-tempered metadynamics: a smoothly converging and tunable free-energy method. *Physical review letters*, 100(2):020603, 2008.
- Batatia, I., Kovacs, D. P., Simm, G., Ortner, C., and Csányi, G. Mace: Higher order equivariant message passing neural networks for fast and accurate force fields. *Advances in neural information processing systems*, 35: 11423–11436, 2022.
- Batzner, S., Musaelian, A., Sun, L., Geiger, M., Mailoa, J. P., Kornbluth, M., Molinari, N., Smidt, T. E., and Kozinsky, B. E (3)-equivariant graph neural networks for data-efficient and accurate interatomic potentials. *Nature communications*, 13(1):2453, 2022.
- Behler, J. and Parrinello, M. Generalized neural-network representation of high-dimensional potential-energy surfaces. *Physical review letters*, 98(14):146401, 2007.
- Blank, T. B., Brown, S. D., Calhoun, A. W., and Doren, D. J. Neural network models of potential energy surfaces. *The Journal of chemical physics*, 103(10):4129–4137, 1995.
- Blessing, D., Richter, L., Berner, J., Malitskiy, E., and Neumann, G. Bridge matching sampler: Scalable sampling via generalized fixed-point diffusion matching. *arXiv preprint arXiv:2603.00530*, 2026.
- Bonomi, M., Branduardi, D., Bussi, G., Camilloni, C., Provasi, D., Raiteri, P., Donadio, D., Marinelli, F., Pietrucci, F., Broglia, R. A., et al. Plumed: A portable plugin for free-energy calculations with molecular dynamics. *Computer Physics Communications*, 180(10): 1961–1972, 2009.
- Chandler, D. *Introduction to Modern Statistical Mechanics*. Oxford University Press, 1987.
- Charron, N. E., Bonneau, K., Pasos-Trejo, A. S., Guljas, A., Chen, Y., Musil, F., Venturin, J., Gusew, D., Zaporozhets, I., Krämer, A., et al. Navigating protein landscapes with a machine-learned transferable coarse-grained model. *Nature Chemistry*, pp. 1–9, 2025.
- Chen, R. T., Rubanova, Y., Bettencourt, J., and Duvenaud, D. K. Neural ordinary differential equations. *Advances in neural information processing systems*, 31, 2018.
- Chen, W. and Ferguson, A. L. Molecular enhanced sampling with autoencoders: On-the-fly collective variable discovery and accelerated free energy landscape exploration. *Journal of computational chemistry*, 39(25):2079–2102, 2018.
- Chen, W., Görlich, F., Fuchs, P., and Zavadlav, J. Enhanced sampling for efficient learning of coarse-grained machine learning potentials. *Journal of Chemical Theory and Computation*, 22(1):219–230, 2026. doi: 10.1021/acs.jctc.5c01712. URL <https://doi.org/10.1021/acs.jctc.5c01712>.
- Chen, Y., Krämer, A., Charron, N. E., Husic, B. E., Clementi, C., and Noé, F. Machine learning implicit

- solvation for molecular dynamics. *The Journal of Chemical Physics*, 155(8):084101, August 2021. ISSN 1089-7690. doi: 10.1063/5.0059915. URL <http://dx.doi.org/10.1063/5.0059915>.
- Chennakesavalu, S., Toomer, D. J., and Rotskoff, G. M. Ensuring thermodynamic consistency with invertible coarse-graining. *The Journal of Chemical Physics*, 158(12), 2023.
- Chipot, C. and Pohorille, A. *Free energy calculations*, volume 86. Springer, 2007.
- Ciccotti, G., Kapral, R., and Vanden-Eijnden, E. Blue moon sampling, vectorial reaction coordinates, and unbiased constrained dynamics. *ChemPhysChem*, 6(9):1809–1814, 2005.
- Costa, A. d. S., Ponnampati, M., Rubin, D., Smidt, T., and Jacobson, J. Accelerating protein molecular dynamics simulation with deepjump. *arXiv preprint arXiv:2509.13294*, 2025.
- Daigavane, A., Vani, B. P., Davidson, D., Saremi, S., Rackers, J. A., and Kleinhenz, J. Jamun: Bridging smoothed molecular dynamics and score-based learning for conformational ensemble generation. In *The Thirty-ninth Annual Conference on Neural Information Processing Systems*, 2025.
- Dibak, M., Klein, L., Krämer, A., and Noé, F. Temperature steerable flows and boltzmann generators, 2022. URL <https://arxiv.org/abs/2108.01590>.
- Didi, K., Zhang, Z., Zhou, G., Reidenbach, D., Cao, Z., Cha, S., Geffner, T., Dallago, C., Tang, J., Bronstein, M. M., et al. Scaling atomistic protein binder design with generative pretraining and test-time compute. *arXiv preprint arXiv:2603.27950*, 2026.
- Diez, J. V., Schreiner, M., and Olsson, S. Transferable generative models bridge femtosecond to nanosecond time-step molecular dynamics. *arXiv preprint arXiv:2510.07589*, 2025.
- Dinh, L., Krueger, D., and Bengio, Y. Nice: Non-linear independent components estimation. *arXiv preprint arXiv:1410.8516*, 2014.
- dos Santos Costa, A., Mitnikov, I., Pellegrini, F., Daigavane, A., Geiger, M., Cao, Z., Kreis, K., Smidt, T., Kucukbenli, E., and Jacobson, J. Equijump: Protein dynamics simulation via so(3)-equivariant stochastic interpolants, 2024.
- Durumeric, A. E., Charron, N. E., Templeton, C., Musil, F., Bonneau, K., Pasos-Trejo, A. S., Chen, Y., Kelkar, A., Noé, F., and Clementi, C. Machine learned coarse-grained protein force-fields: Are we there yet? *Current opinion in structural biology*, 79:102533, 2023.
- Durumeric, A. E., Chen, Y., Noé, F., and Clementi, C. Learning data efficient coarse-grained molecular dynamics from forces and noise. *arXiv preprint arXiv:2407.01286*, 2024.
- Eastman, P., Galvelis, R., Peláez, R. P., Abreu, C. R., Farr, S. E., Gallicchio, E., Gorenko, A., Henry, M. M., Hu, F., Huang, J., et al. Openmm 8: molecular dynamics simulation with machine learning potentials. *The Journal of Physical Chemistry B*, 128(1):109–116, 2023.
- Fan, Z., Zhang, W., Zhang, Z., Xu, K., Shao, X., and Dong, H. Nep-cg and nep-aacg: Efficient coarse-grained and multiscale all-atom-coarse-grained neuroevolution potentials. *Computational Materials Today*, 10:100055, 2026.
- Frenkel, D. and Smit, B. *Understanding Molecular Simulation*. Elsevier, 2002. doi: 10.1016/b978-0-12-267351-1.x5000-7. URL <https://doi.org/10.1016/b978-0-12-267351-1.x5000-7>.
- Fuchs, P. and Zavadlav, J. Refining machine learning potentials through thermodynamic theory of phase transitions. *arXiv preprint arXiv:2512.03974*, 2025.
- Fuchs, P., Chen, W., Thaler, S., and Zavadlav, J. chemtrain-deploy: A parallel and scalable framework for machine learning potentials in million-atom md simulations. *Journal of Chemical Theory and Computation*, 21(15):7550–7560, 2025a.
- Fuchs, P., Thaler, S., Röcken, S., and Zavadlav, J. chemtrain: Learning deep potential models via automatic differentiation and statistical physics. *Computer Physics Communications*, 310:109512, 2025b.
- Gloy, J. F. and Olsson, S. Hollowflow: Efficient sample likelihood evaluation using hollow message passing. *arXiv preprint arXiv:2510.21542*, 2025.
- Görlich, F. and Zavadlav, J. Mapping still matters: Coarse-graining with machine learning potentials. *arXiv preprint arXiv:2512.07692*, 2025.
- Havens, A., Miller, B. K., Yan, B., Domingo-Enrich, C., Sriram, A., Wood, B., Levine, D., Hu, B., Amos, B., Karrer, B., et al. Adjoint sampling: Highly scalable diffusion samplers via adjoint matching. *arXiv preprint arXiv:2504.11713*, 2025.
- Hawkins, G. D., Cramer, C. J., and Truhlar, D. G. Pairwise solute descreening of solute charges from a dielectric medium. *Chemical Physics Letters*, 246(1-2):122–129, 1995.

- He, J., Du, Y., Vargas, F., Zhang, D., Padhy, S., OuYang, R., Gomes, C., and Hernández-Lobato, J. M. No trick, no treat: Pursuits and challenges towards simulation-free training of neural samplers. *arXiv preprint arXiv:2502.06685*, 2025.
- Heek, J., Levskaya, A., Oliver, A., Ritter, M., Rondepierre, B., Steiner, A., and van Zee, M. Flax: A neural network library and ecosystem for JAX, 2024. URL <http://github.com/google/flax>.
- Hénin, J., Lelièvre, T., Shirts, M. R., Valsson, O., and Delemotte, L. Enhanced sampling methods for molecular dynamics simulations [article v1.0]. *Living Journal of Computational Molecular Science*, 4(1), 2022. doi: 10.33011/livecoms.4.1.1583. URL <https://doi.org/10.33011/livecoms.4.1.1583>.
- Herringer, N. S., Dasetty, S., Gandhi, D., Lee, J., and Ferguson, A. L. Permutationally invariant networks for enhanced sampling (pines): Discovery of multimolecular and solvent-inclusive collective variables. *Journal of Chemical Theory and Computation*, 20(1):178–198, 2023.
- Hummerich, S., Bereau, T., and Köthe, U. Split-flows: Measure transport and information loss across molecular resolutions. *arXiv preprint arXiv:2511.01464*, 2025.
- Hutchinson, M. F. A stochastic estimator of the trace of the influence matrix for laplacian smoothing splines. *Communications in Statistics-Simulation and Computation*, 18(3):1059–1076, 1989.
- Invernizzi, M., Kramer, A., Clementi, C., and Noé, F. Skipping the replica exchange ladder with normalizing flows. *The Journal of Physical Chemistry Letters*, 13(50):11643–11649, 2022.
- Janson, G. and Feig, M. Generation of protein dynamics by machine learning. *Current Opinion in Structural Biology*, 93:103115, 2025.
- Jin, J., Pak, A. J., Durumeric, A. E. P., Loose, T. D., and Voth, G. A. Bottom-up Coarse-Graining: Principles and Perspectives. *Journal of Chemical Theory and Computation*, 18(10):5759–5791, October 2022. ISSN 1549-9618. doi: 10.1021/acs.jctc.2c00643.
- Jing, B., Berger, B., and Jaakkola, T. AlphaFold meets flow matching for generating protein ensembles. *arXiv preprint arXiv:2402.04845*, 2024.
- Kabylda, A., Frank, J. T., Suárez-Dou, S., Khabibrakhmanov, A., Medrano Sandonas, L., Unke, O. T., Chmiela, S., Müller, K.-R., and Tkatchenko, A. Molecular simulations with a pretrained neural network and universal pairwise force fields. *Journal of the American Chemical Society*, 147(37):33723–33734, 2025.
- Kidger, P. *On Neural Differential Equations*. PhD thesis, University of Oxford, 2021.
- Kish, L. *Survey Sampling*. John Wiley & Sons, Inc, New York, 1965.
- Klein, L. and Noé, F. Transferable boltzmann generators. *Advances in Neural Information Processing Systems*, 37: 45281–45314, 2024.
- Klein, L., Foong, A. Y. K., Fjelde, T. E., Mlodozieniec, B., Brockschmidt, M., Nowozin, S., Noé, F., and Tomioka, R. Timewarp: Transferable acceleration of molecular dynamics by learning time-coarsened dynamics, 2023. URL <https://arxiv.org/abs/2302.01170>.
- Köhler, J., Klein, L., and Noé, F. Equivariant flows: Exact likelihood generative learning for symmetric densities. In III, H. D. and Singh, A. (eds.), *Proceedings of the 37th International Conference on Machine Learning*, volume 119 of *Proceedings of Machine Learning Research*, pp. 5361–5370. PMLR, 13–18 Jul 2020. URL <https://proceedings.mlr.press/v119/kohler20a.html>.
- Kohler, J., Chen, Y., Kramer, A., Clementi, C., and Noé, F. Flow-matching: Efficient coarse-graining of molecular dynamics without forces. *Journal of Chemical Theory and Computation*, 19(3):942–952, 2023.
- Krishna, V., Noid, W. G., and Voth, G. A. The multiscale coarse-graining method. iv. transferring coarse-grained potentials between temperatures. *The Journal of chemical physics*, 131(2), 2009.
- Laio, A. and Gervasio, F. L. Metadynamics: a method to simulate rare events and reconstruct the free energy in biophysics, chemistry and material science. *Reports on Progress in Physics*, 71(12):126601, 2008.
- Lewis, S., Hempel, T., Jiménez-Luna, J., Gastegger, M., Xie, Y., Foong, A. Y., Satorras, V. G., Abdin, O., Veeling, B. S., Zaporozhets, I., et al. Scalable emulation of protein equilibrium ensembles with generative deep learning. *Science*, pp. eadv9817, 2025.
- Lindorff-Larsen, K., Piana, S., Palmo, K., Maragakis, P., Klepeis, J. L., Dror, R. O., and Shaw, D. E. Improved side-chain torsion potentials for the amber ff99sb protein force field. *Proteins: Structure, Function, and Bioinformatics*, 78(8):1950–1958, 2010.
- Lindorff-Larsen, K., Piana, S., Dror, R. O., and Shaw, D. E. How fast-folding proteins fold. *Science*, 334(6055):517–520, 2011.

- Lipman, Y., Chen, R. T., Ben-Hamu, H., Nickel, M., and Le, M. Flow matching for generative modeling. *arXiv preprint arXiv:2210.02747*, 2022.
- Liu, G.-H., Choi, J., Chen, Y., Miller, B. K., and Chen, R. T. Adjoint schrödinger bridge sampler. *arXiv preprint arXiv:2506.22565*, 2025.
- Liu, X., Gong, C., and Liu, Q. Flow straight and fast: Learning to generate and transfer data with rectified flow, 2022. URL <https://arxiv.org/abs/2209.03003>.
- Majewski, M., Pérez, A., Thölke, P., Doerr, S., Charron, N. E., Giorgino, T., Husic, B. E., Clementi, C., Noé, F., and De Fabritiis, G. Machine learning coarse-grained potentials of protein thermodynamics. *Nature Communications*, 14(1), September 2023. ISSN 2041-1723. doi: 10.1038/s41467-023-41343-1. URL <http://dx.doi.org/10.1038/s41467-023-41343-1>.
- Marrink, S. J., Risselada, H. J., Yefimov, S., Tieleman, D. P., and De Vries, A. H. The martini force field: coarse grained model for biomolecular simulations. *The journal of physical chemistry B*, 111(27):7812–7824, 2007.
- Mehdi, S., Smith, Z., Herron, L., Zou, Z., and Tiwary, P. Enhanced sampling with machine learning. *Annual Review of Physical Chemistry*, 75(2024):347–370, 2024.
- Midgley, L. I., Stimper, V., Simm, G. N. C., Schölkopf, B., and Hernández-Lobato, J. M. Flow annealed importance sampling bootstrap, 2023. URL <https://arxiv.org/abs/2208.01893>.
- Mirarchi, A., Peláez, R. P., Simeon, G., and De Fabritiis, G. Amaro: All heavy-atom transferable neural network potentials of protein thermodynamics. *Journal of Chemical Theory and Computation*, 20(22):9871–9878, 2024.
- Moqvist, S., Chen, W., Schreiner, M., N’uske, F., and Olsson, S. Thermodynamic interpolation: A generative approach to molecular thermodynamics and kinetics. *Journal of Chemical Theory and Computation*, 21(5):2535–2545, 2025.
- Musil, F., Willatt, M. J., Langovoy, M. A., and Ceriotti, M. Fast and accurate uncertainty estimation in chemical machine learning. *Journal of chemical theory and computation*, 15(2):906–915, 2019.
- Nam, J., Máté, B., Toshev, A. P., Kaniselman, M., Gómez-Bombarelli, R., Chen, R. T., Wood, B., Liu, G.-H., and Miller, B. K. Enhancing diffusion-based sampling with molecular collective variables. *arXiv preprint arXiv:2510.11923*, 2025.
- Nguyen, H., Roe, D. R., and Simmerling, C. Improved generalized born solvent model parameters for protein simulations. *Journal of chemical theory and computation*, 9(4):2020–2034, 2013.
- Noé, F., Olsson, S., Köhler, J., and Wu, H. Boltzmann generators: Sampling equilibrium states of many-body systems with deep learning. *Science*, 365(6457):eaaw1147, 2019.
- Noid, W. G. Perspective: Coarse-grained models for biomolecular systems. *The Journal of Chemical Physics*, 139(9):090901, September 2013. ISSN 0021-9606. doi: 10.1063/1.4818908.
- Noid, W. G., Chu, J.-W., Ayton, G. S., Krishna, V., Izvekov, S., Voth, G. A., Das, A., and Andersen, H. C. The multiscale coarse-graining method. i. a rigorous bridge between atomistic and coarse-grained models. *The Journal of chemical physics*, 128(24), 2008.
- Olsson, S. Generative molecular dynamics. *Current Opinion in Structural Biology*, 96:103213, 2026.
- Onufriev, A., Bashford, D., and Case, D. A. Exploring protein native states and large-scale conformational changes with a modified generalized born model. *Proteins: Structure, Function, and Bioinformatics*, 55(2):383–394, 2004.
- OuYang, R., Grenioux, L., and Hernández-Lobato, J. M. A diffusive classification loss for learning energy-based generative models. *arXiv preprint arXiv:2601.21025*, 2026.
- Park, A., Chennakesavalu, S., and Rotskoff, G. M. Scaling transferable coarse-graining with mean force matching. *arXiv preprint arXiv:2602.14531*, 2026.
- Peng, X. and Gao, A. Flow perturbation to accelerate boltzmann sampling. *Nature Communications*, 16(1):6604, 2025.
- Plainer, M., Wu, H., Klein, L., Günnemann, S., and Noé, F. Consistent sampling and simulation: Molecular dynamics with energy-based diffusion models. *arXiv preprint arXiv:2506.17139*, 2025.
- Potapchik, P., Lee, C.-K., and Albergo, M. S. Tilt matching for scalable sampling and fine-tuning. *arXiv preprint arXiv:2512.21829*, 2025.
- Raja, S., Šípka, M., Psenka, M., Kreiman, T., Pavelka, M., and Krishnapriyan, A. S. Action-minimization meets generative modeling: Efficient transition path sampling with the onsager-machlup functional. *arXiv preprint arXiv:2504.18506*, 2025.
- Ramachandran, G. N. Stereochemistry of polypeptide chain configurations. *J. Mol. Biol.*, 7:95–99, 1963.

- Rehman, D., Akhound-Sadegh, T., Gazizov, A., Bengio, Y., and Tong, A. Falcon: Few-step accurate likelihoods for continuous flows. *arXiv preprint arXiv:2512.09914*, 2025.
- Rehman, D., Tan, C. B., Bengio, Y., Bose, J., and Tong, A. Autoregressive boltzmann generators. *ICLR 2026 Workshop on Generative and Experimental Perspectives for Biomolecular Design*, 2026. URL <https://openreview.net/forum?id=tyQ3hBeY7L>.
- Rezende, D. J. and Mohamed, S. Variational inference with normalizing flows, 2016.
- Ribeiro, J. M. L., Bravo, P., Wang, Y., and Tiwary, P. Reweighted autoencoded variational bayes for enhanced sampling (rave). *The Journal of chemical physics*, 149(7), 2018.
- Rotskoff, G. M. Sampling thermodynamic ensembles of molecular systems with generative neural networks: Will integrating physics-based models close the generalization gap? *Current Opinion in Solid State and Materials Science*, 30:101158, 2024.
- Saunders, M. G. and Voth, G. A. Coarse-graining methods for computational biology. *Annual review of biophysics*, 42(1):73–93, 2013.
- Schebek, M. and Rogal, J. Scalable boltzmann generators for equilibrium sampling of large-scale materials. *arXiv preprint arXiv:2509.25486*, 2025.
- Schoenholz, S. and Cubuk, E. D. Jax md: a framework for differentiable physics. *Advances in Neural Information Processing Systems*, 33:11428–11441, 2020.
- Schopmans, H. and Friederich, P. Conditional normalizing flows for active learning of coarse-grained molecular representations. In *International Conference on Machine Learning*, pp. 43804–43827. PMLR, 2024.
- Schreiner, M., Winther, O., and Olsson, S. Implicit transfer operator learning: Multiple time-resolution models for molecular dynamics. *Advances in Neural Information Processing Systems*, 36:36449–36462, 2023.
- Shell, M. S. The relative entropy is fundamental to multi-scale and inverse thermodynamic problems. *The Journal of chemical physics*, 129(14), 2008.
- Shi, Y., Huang, Z., Feng, S., Zhong, H., Wang, W., and Sun, Y. Masked label prediction: Unified message passing model for semi-supervised classification. *arXiv preprint arXiv:2009.03509*, 2020.
- Souza, P. C., Alessandri, R., Barnoud, J., Thallmair, S., Faustino, I., Grünewald, F., Patmanidis, I., Abdizadeh, H., Bruininks, B. M., Wassenaar, T. A., et al. Martini 3: a general purpose force field for coarse-grained molecular dynamics. *Nature methods*, 18(4):382–388, 2021.
- Stukowski, A. Visualization and analysis of atomistic simulation data with ovito—the open visualization tool. *Modelling and simulation in materials science and engineering*, 18(1):015012, 2009.
- Stupp, M. and Koutsourelakis, P. Energy-based coarse-graining in molecular dynamics: A flow-based framework without data. *arXiv preprint arXiv:2504.20940*, 2025.
- Tamagnone, S., Laio, A., and Gabrié, M. Coarse-grained molecular dynamics with normalizing flows. *Journal of Chemical Theory and Computation*, 20(18):7796–7805, 2024.
- Tan, C. B., Bose, A. J., Lin, C., Klein, L., Bronstein, M. M., and Tong, A. Scalable equilibrium sampling with sequential boltzmann generators. *arXiv preprint arXiv:2502.18462*, 2025a.
- Tan, C. B., Hassan, M., Klein, L., Syed, S., Beaini, D., Bronstein, M. M., Tong, A., and Neklyudov, K. Amortized sampling with transferable normalizing flows. *arXiv preprint arXiv:2508.18175*, 2025b.
- Thaler, S. and Zavadlav, J. Learning neural network potentials from experimental data via differentiable trajectory reweighting. *Nature communications*, 12(1):6884, 2021.
- Thaler, S., Stupp, M., and Zavadlav, J. Deep coarse-grained potentials via relative entropy minimization. *The Journal of Chemical Physics*, 157(24):244103, December 2022. ISSN 0021-9606. doi: 10.1063/5.0124538.
- Tong, A., Fatras, K., Malkin, N., Huguet, G., Zhang, Y., Rector-Brooks, J., Wolf, G., and Bengio, Y. Improving and generalizing flow-based generative models with mini-batch optimal transport. *arXiv preprint arXiv:2302.00482*, 2023.
- Torrie, G. and Valleau, J. Nonphysical sampling distributions in monte carlo free-energy estimation: Umbrella sampling. *Journal of Computational Physics*, 23(2):187–199, February 1977. doi: 10.1016/0021-9991(77)90121-8. URL [https://doi.org/10.1016/0021-9991\(77\)90121-8](https://doi.org/10.1016/0021-9991(77)90121-8).
- Unke, O. T., Chmiela, S., Sauceda, H. E., Gastegger, M., Poltavsky, I., Schütt, K. T., Tkatchenko, A., and Müller, K.-R. Machine learning force fields. *Chemical Reviews*, 121(16):10142–10186, 2021.
- Van Der Spoel, D., Lindahl, E., Hess, B., Groenhof, G., Mark, A. E., and Berendsen, H. J. Gromacs: fast, flexible, and free. *Journal of computational chemistry*, 26(16):1701–1718, 2005.

- Vempala, S. and Wibisono, A. Rapid convergence of the unadjusted langevin algorithm: Isoperimetry suffices. *Advances in neural information processing systems*, 32, 2019.
- Vlachas, P. R., Zavadlav, J., Praprotnik, M., and Koumoutsakos, P. Accelerated simulations of molecular systems through learning of effective dynamics. *Journal of Chemical Theory and Computation*, 18(1):538–549, 2021.
- von Klitzing, C., Blessing, D., Schopmans, H., Friederich, P., and Neumann, G. Learning boltzmann generators via constrained mass transport. *arXiv preprint arXiv:2510.18460*, 2025.
- Wang, J., Olsson, S., Wehmeyer, C., Pérez, A., Charron, N. E., De Fabritiis, G., Noé, F., and Clementi, C. Machine learning of coarse-grained molecular dynamics force fields. *ACS central science*, 5(5):755–767, 2019.
- Wang, W., Xu, M., Cai, C., Miller, B. K., Smidt, T., Wang, Y., Tang, J., and Gómez-Bombarelli, R. Generative coarse-graining of molecular conformations. *arXiv preprint arXiv:2201.12176*, 2022.
- Wirnsberger, P., Ballard, A. J., Papamakarios, G., Abercrombie, S., Racanière, S., Pritzel, A., Jimenez Rezende, D., and Blundell, C. Targeted free energy estimation via learned mappings. *The Journal of Chemical Physics*, 153(14), October 2020. ISSN 1089-7690. doi: 10.1063/5.0018903. URL <http://dx.doi.org/10.1063/5.0018903>.
- Wood, B. M., Dzamba, M., Fu, X., Gao, M., Shuaibi, M., Barroso-Luque, L., Abdelmaqsoud, K., Gharakhanyan, V., Kitchin, J. R., Levine, D. S., et al. Uma: A family of universal models for atoms. *arXiv preprint arXiv:2506.23971*, 2025.
- Xie, Y., Winkler, L., Sun, L., Lewis, S., Foster, A. E., Luna, J. J., Hempel, T., Gastegger, M., Chen, Y., Zaporozhets, I., et al. Enhanced diffusion sampling: Efficient rare event sampling and free energy calculation with diffusion models. *arXiv preprint arXiv:2602.16634*, 2026.
- Xu, Y., Wang, D., Zhou, Z., Yu, T., and Chen, M. Tempo: Temporal multi-scale autoregressive generation of protein conformational ensembles. *arXiv preprint arXiv:2511.05510*, 2025.
- Yu, Z., He, Y., Huang, W., Yan, W., and Liu, Y. Card: Coarse-to-fine autoregressive modeling with radix-based decomposition for transferable free energy estimation. *arXiv preprint arXiv:2605.02657*, 2026.
- Zaverkin, V., Holzmüller, D., Christiansen, H., Errica, F., Alesiani, F., Takamoto, M., Niepert, M., and Kästner, J. Uncertainty-biased molecular dynamics for learning uniformly accurate interatomic potentials. *npj Computational Materials*, 10(1):83, 2024.
- Zhai, S., Zhang, R., Nakkiran, P., Berthelot, D., Gu, J., Zheng, H., Chen, T., Bautista, M. A., Jaitly, N., and Susskind, J. Normalizing flows are capable generative models. *arXiv preprint arXiv:2412.06329*, 2024.
- Zhang, L., Han, J., Wang, H., Car, R., and E, W. DeePCG: Constructing coarse-grained models via deep neural networks. *The Journal of Chemical Physics*, 149(3): 034101, July 2018. ISSN 0021-9606, 1089-7690. doi: 10.1063/1.5027645.
- Zhang, M., Zhang, Z., Wu, H., and Wang, Y. Flow matching for optimal reaction coordinates of biomolecular systems. *Journal of Chemical Theory and Computation*, 21(1): 399–412, 2024.
- Zheng, S., He, J., Liu, C., Shi, Y., Lu, Z., Feng, W., Ju, F., Wang, J., Zhu, J., Min, Y., et al. Predicting equilibrium distributions for molecular systems with deep learning. *Nature Machine Intelligence*, 6(5):558–567, 2024.
- Zhu, J., Bülow, S. v., Liu, H., Lindorff-Larsen, K., and Chen, H. Extending conformational ensemble prediction to multidomain proteins and protein complex. *bioRxiv*, pp. 2026–01, 2026.
- Zhu, K., Trizio, E., Zhang, J., Hu, R., Jiang, L., Hou, T., and Bonati, L. Enhanced sampling in the age of machine learning: Algorithms and applications. *Chemical Reviews*, 2025.

A. Proofs

A.1. Proof of Proposition 1

Proposition 1. Let $p^*(\mathbf{R}) \propto e^{-\beta U^*(\mathbf{R})}$ be the true marginal and $p_\eta(\mathbf{R}) \propto e^{-\beta U_\eta(\mathbf{R})}$ the learned distribution. If p^* satisfies a Logarithmic Sobolev Inequality (LSI) with constant $\rho > 0$. Then, the Kullback-Leibler divergence between the learned and true distributions is bounded by the expected squared force error:

$$\mathcal{D}_{\text{KL}}(p_\eta \| p^*) \leq \frac{\beta^2}{2\rho} \mathbb{E}_{p_\eta} [\|\nabla U_\eta(\mathbf{R}) - \nabla U^*(\mathbf{R})\|^2]. \quad (14)$$

Proof. The Kullback-Leibler divergence is defined as:

$$\mathcal{D}_{\text{KL}}(p_\eta \| p^*) = \int p_\eta(\mathbf{R}) \log \frac{p_\eta(\mathbf{R})}{p^*(\mathbf{R})} d\mathbf{R}. \quad (19)$$

The Fisher Divergence (or relative Fisher information) between p_η and p^* is defined as:

$$\mathcal{J}(p_\eta \| p^*) = \int p_\eta(\mathbf{R}) \|\nabla \log p_\eta(\mathbf{R}) - \nabla \log p^*(\mathbf{R})\|^2 d\mathbf{R}. \quad (20)$$

Since $p_\eta(\mathbf{R}) = Z_\eta^{-1} e^{-\beta U_\eta(\mathbf{R})}$ and $p^*(\mathbf{R}) = (Z^*)^{-1} e^{-\beta U^*(\mathbf{R})}$, the gradients of the log-densities are directly proportional to the forces:

$$\nabla \log p_\eta(\mathbf{R}) = -\beta \nabla U_\eta(\mathbf{R}), \quad \nabla \log p^*(\mathbf{R}) = -\beta \nabla U^*(\mathbf{R}). \quad (21)$$

Substituting these into the definition of the Fisher Divergence:

$$\mathcal{J}(p_\eta \| p^*) = \int p_\eta(\mathbf{R}) \|(-\beta \nabla U_\eta(\mathbf{R})) - (-\beta \nabla U^*(\mathbf{R}))\|^2 d\mathbf{R} \quad (22)$$

$$= \beta^2 \int p_\eta(\mathbf{R}) \|\nabla U_\eta(\mathbf{R}) - \nabla U^*(\mathbf{R})\|^2 d\mathbf{R} \quad (23)$$

$$= \beta^2 \mathbb{E}_{p_\eta} [\|\mathcal{F}_\eta(\mathbf{R}) - \mathcal{F}^*(\mathbf{R})\|^2]. \quad (24)$$

We assume that the target distribution p^* satisfies a Logarithmic Sobolev Inequality (LSI) with constant $\rho > 0$. By definition, this inequality implies that for any distribution p_η absolutely continuous with respect to p^* :

$$\mathcal{D}_{\text{KL}}(p_\eta \| p^*) \leq \frac{1}{2\rho} \mathcal{J}(p_\eta \| p^*). \quad (25)$$

Substituting our expression for the Fisher Divergence into the LSI yields the final bound:

$$\mathcal{D}_{\text{KL}}(p_\eta \| p^*) \leq \frac{1}{2\rho} (\beta^2 \mathbb{E}_{p_\eta} [\|\nabla U_\eta(\mathbf{R}) - \nabla U^*(\mathbf{R})\|^2]). \quad (26)$$

Dividing out the constants concludes the proof. \square

A.2. Proof of Proposition 2

Proposition 2. (Chen et al. (2026)) Let $V(\mathbf{R})$ be a bias potential depending only on the coarse-grained coordinates. The conditional distribution of atomistic configurations given \mathbf{R} is invariant:

$$p_V(\mathbf{r} | \mathbf{R}) = p(\mathbf{r} | \mathbf{R}). \quad (15)$$

Proof. Let $p(\mathbf{r}) = Z^{-1} e^{-\beta u(\mathbf{r})}$ be the unbiased equilibrium distribution. By definition, the unbiased marginal distribution is

$$p(\mathbf{R}) = \int p(\mathbf{r}) \delta(\Xi(\mathbf{r}) - \mathbf{R}) d\mathbf{r} = \frac{1}{Z} \int e^{-\beta u(\mathbf{r})} \delta(\Xi(\mathbf{r}) - \mathbf{R}) d\mathbf{r}. \quad (27)$$

Rearranging this yields the identity for the unnormalized marginal:

$$\int e^{-\beta u(\mathbf{r})} \delta(\Xi(\mathbf{r}) - \mathbf{R}) d\mathbf{r} = Zp(\mathbf{R}). \quad (28)$$

Now, consider the biased distribution $p_V(\mathbf{r}) = Z_V^{-1} e^{-\beta(u(\mathbf{r})+V(\Xi(\mathbf{r})))}$. The biased marginal distribution is:

$$p_V(\mathbf{R}) = \int \frac{e^{-\beta u(\mathbf{r})} e^{-\beta V(\Xi(\mathbf{r}))}}{Z_V} \delta(\Xi(\mathbf{r}) - \mathbf{R}) d\mathbf{r} \quad (29)$$

$$= \frac{e^{-\beta V(\mathbf{R})}}{Z_V} \underbrace{\int e^{-\beta u(\mathbf{r})} \delta(\Xi(\mathbf{r}) - \mathbf{R}) d\mathbf{r}}_{=Zp(\mathbf{R}) \text{ (from Eq. 28)}} \quad (30)$$

$$= \frac{Z}{Z_V} e^{-\beta V(\mathbf{R})} p(\mathbf{R}). \quad (31)$$

Finally, substituting this into the definition of the conditional distribution:

$$p_V(\mathbf{r} | \mathbf{R}) = \frac{p_V(\mathbf{r}) \delta(\Xi(\mathbf{r}) - \mathbf{R})}{p_V(\mathbf{R})} = \frac{Z_V^{-1} e^{-\beta u(\mathbf{r})} e^{-\beta V(\mathbf{R})} \delta(\dots)}{\frac{Z}{Z_V} e^{-\beta V(\mathbf{R})} p(\mathbf{R})} = \frac{e^{-\beta u(\mathbf{r})} \delta(\dots)}{Zp(\mathbf{R})} = p(\mathbf{r} | \mathbf{R}). \quad (32)$$

□

B. Datasets

B.1. Müller-Brown Potential

Potential Parameters. For the two-dimensional toy system, we use a Müller-Brown potential defined as

$$u(x, y) = u_1(x, y) + u_2(x, y) + u_3(x, y) + u_4(x, y), \quad (33)$$

with (Raja et al., 2025)

$$\begin{aligned} u_1(x, y) &= -17.3 \exp[-0.0039(x - 48)^2 - 0.0391(y - 8)^2], \\ u_2(x, y) &= -8.7 \exp[-0.0039(x - 32)^2 - 0.0391(y - 16)^2], \\ u_3(x, y) &= -14.7 \exp[-0.0254(x - 24)^2 + 0.043(x - 24)(y - 32) - 0.0254(y - 32)^2], \\ u_4(x, y) &= 1.3 \exp[0.00273(x - 16)^2 + 0.0023(x - 16)(y - 24) + 0.00273(y - 24)^2]. \end{aligned}$$

Umbrella Sampling. For umbrella sampling, we introduce a biasing potential along the x coordinate,

$$V_x(x) = -4 \exp\left[-\frac{(x - 32.0)^2}{2 \cdot 5^2}\right].$$

This enables better sampling of the configurations around $\mathbf{x}_0 = 32$, allowing a better representation of transition regions that are otherwise rarely visited in unbiased trajectories.

Simulation Details. For the MB dataset generation, we perform two-dimensional Langevin dynamics with a time step of 0.1, mass $m = 1.0$, friction coefficient $\gamma = 0.1$, and temperature $k_B T = 1.0$. Ten independent trajectories of length 10^7 steps are generated, with initial positions sampled uniformly from $[10, 50]^2$ and initial velocities drawn from a Gaussian distribution with standard deviation 0.1. Configurations are recorded every 10 steps. The dynamics follow

$$m\ddot{\mathbf{r}} = -\nabla(u(\mathbf{r}) + V(x)) - \gamma m\dot{\mathbf{r}} + \sqrt{2\gamma k_B T m} \boldsymbol{\eta}(t), \quad (34)$$

where $V(x)$ is the applied bias, and $\boldsymbol{\eta}(t)$ denotes Gaussian white noise. For each saved configuration, unbiased forces from ∇u are computed and stored.

B.2. Alanine Peptides

Force Fields. For the explicit solvent dataset, alanine peptide systems are parameterized using the AMBER99SB-ILDN force field (Lindorff-Larsen et al., 2010) and solvated in a cubic box of TIP3P water molecules. Explicit solvent simulations of alanine dipeptide are carried out with GROMACS (Van Der Spoel et al., 2005), while all remaining peptide systems are simulated using OpenMM (Eastman et al., 2023). For implicit solvent, the same force field is used together with the generalized Born (OBC1/OBC2) model, and all simulations are performed using OpenMM.

Well-Tempered Metadynamics. We perform well-tempered metadynamics (WT-MetaD) (Barducci et al., 2008) simulations of alanine peptides in explicit solvent using GROMACS coupled with PLUMED (Bonomi et al., 2009). The backbone dihedral angles ϕ (C–N–C $_{\alpha}$ –C) and ψ (N–C $_{\alpha}$ –C–N) are chosen as collective variables. Gaussian hills with height 1.2 kJ/mol and width 0.35 rad are deposited every 500 integration steps. Datasets are generated with bias factors $\gamma = 1.5$ and $\gamma = 9$, where $\gamma = 1.5$ is used to train flow model for biased dipeptide proposal generation and $\gamma = 9$ is used for enhanced sampling force matching. Positions and forces are recorded. To ensure unbiased force labels, all forces are recomputed by rerunning the saved trajectories in GROMACS without the metadynamics bias using the `mdrun -rerun` functionality. This guarantees that each configuration is associated with forces from the underlying unbiased potential.

For WT-MetaD, the backbone dihedral pair (ϕ, ψ) is used as collective variables for the dipeptide system. For the tripeptide and hexapeptide systems, biasing is applied only to the specific dihedral pair of interest, which is the second pair (of three) for alanine tripeptide and the third pair (of six) for alanine hexapeptide, counting from the N-methyl terminus. As a result, convergence is primarily enforced along the targeted collective variables, which we find sufficient for accurate estimation of the PMF along the corresponding degrees of freedom in this work. More general biasing schemes or longer simulations may further improve sampling of the remaining degrees of freedom, and thereby improve the accuracy of the global PMF.

Simulation Details. All simulations are performed in the NVT ensemble at a temperature of 300 K, with a time step of 0.5 fs and no bond constraints. After energy minimization, production dynamics are carried out using a velocity-rescale thermostat (time constant 0.1 ps). Long-range electrostatics are treated using the particle mesh Ewald method, and van der Waals interactions are truncated at 1.0 nm. We summarize the dataset configurations used in this work in Tab. 4.

Table 4. Overview of simulation details for alanine peptide datasets.

System	Solvent	Dataset	Method	Length
Dipeptide	Explicit (TIP3P)	Unbiased MD	None	500 ns
	Explicit (TIP3P)	Biased MD (CNF)	WT-MetaD ($\gamma = 1.5$)	10 ns
	Explicit (TIP3P)	Biased MD (PMF)	WT-MetaD ($\gamma = 9$)	10 ns
	Implicit (OBC1)	Unbiased MD	None	500 ns
	Implicit (OBC2)	Unbiased MD	None	500 ns
Tripeptide	Explicit (TIP3P)	Unbiased MD	None	1000 ns
	Explicit (TIP3P)	Biased MD (PMF)	WT-MetaD ($\gamma = 9$)	50 ns
	Implicit (OBC2)	Unbiased MD	None	1500 ns
Hexapeptide	Explicit (TIP3P)	Unbiased MD	None	1500 ns
	Explicit (TIP3P)	Biased MD (PMF)	WT-MetaD ($\gamma = 9$)	100 ns
	Implicit (OBC2)	Unbiased MD	None	1500 ns

C. Experimental Details for Conditional Normalizing Flows

C.1. Architecture

Müller-Brown Potential. For MB potential, we use a multilayer perceptron augmented with time conditioning for flow matching. The network consists of three hidden layers with width 96. Flow time is embedded into a 16-dimensional time embedding and concatenated with the input.

Alanine Peptides. For peptides, we use an adapted Graph Transformer architecture (Plainer et al., 2025; Arts et al., 2023;

Shi et al., 2020). Given bead positions \mathbf{x}_i and bead features \mathbf{h}_i , edge attributes are constructed as

$$\mathbf{d}_{ij} = \mathbf{x}_i - \mathbf{x}_j, \quad r_{ij} = \|\mathbf{d}_{ij}\|, \quad \mathbf{e}_{ij} = [\mathbf{d}_{ij}, r_{ij}], \quad (35)$$

and node attributes are initialized as

$$\mathbf{n}_i^{(0)} = [\mathbf{h}_i, \mathbf{x}_i, t], \quad (36)$$

where t denotes the flow time. The bead features and time are embedded into 16- and 4-dimensional vectors, respectively, concatenated with positions, and projected to 128-dimensional node embeddings via a linear layer. Edge attributes are also embedded into 128 dimensions. The model consists of three Graph Transformer layers with 8 attention heads and a head dimension of 64. To enforce rotational equivariance, random global rotations are applied to molecular configurations during training as data augmentation (Abramson et al., 2024). Additionally, translational equivariance is guaranteed by moving the center of mass to the origin and adding noise to the center of mass to lift the data dimensionality back. (Tan et al., 2025a).

C.2. Training Configuration

All models are trained using AdamW with weight decay 10^{-5} and a cosine learning-rate schedule decreasing from 3×10^{-4} to 1×10^{-5} . For the Müller–Brown potential, training is performed for 1000 epochs with batch size 256 using 20k training samples. For alanine dipeptide, models are trained for 5000 epochs with batch size 1024 using 50k samples. For alanine tripeptide and hexapeptide, models are trained for 10000 epochs with batch size 1024 using 200k samples. We find no consistent benefit from exponential moving average (EMA) of model parameters and therefore do not employ it in our experiments.

C.3. Inference

As Hutchinson’s trace estimator introduces bias for BGs (Tan et al., 2025a; Peng & Gao, 2025), we compute the divergence exactly using automatic differentiation. For inference, we use the Dormand–Prince 5(4) method (`dopri5`) with absolute and relative tolerances set to 10^{-5} . Inference is performed with a batch size of 500.

C.4. Computational Cost

The reported inference times (Tab. 5) correspond to generating 10^4 samples. All other training and inference parameters are provided in §C.2 and §C.3.

Table 5. Training and inference time for CFM across different systems and settings. Inference times correspond to 10^4 generated samples. Results marked with \dagger are taken from (Rehman et al., 2025) and are included for reference. Reported runtimes should be interpreted in light of differences in hardware, implementation details, and training and inference batch sizes. Note also that peptide nomenclature differs between the two works due to different conventions for counting terminal capping groups: our alanine tripeptide and hexapeptide correspond to the alanine tetrapeptide and heptapeptide systems reported in (Rehman et al., 2025), respectively.

Model	Alanine Dipeptide			Alanine Tripeptide		
	Training	Inference	Total	Training	Inference	Total
Core Beta	0.45h	0.95min	0.47h	7.32h	6.47min	7.43h
Heavy Atom	0.80h	3.78min	0.86h	17.63h	14.22min	17.87h
All Atom	2.55h	14.91min	2.80h	—	—	—
ECNF++ \dagger	—	—	12.52h	—	—	32.17h
SBG \dagger	—	—	16.83h	—	—	41.67h
DiT CNF \dagger	—	—	9.56h	—	—	24.10h
FALCON \dagger	—	—	7.65h	—	—	25.76h

Model	Alanine Hexapeptide		
	Training	Inference	Total
Core Beta	23.01h	20.07min	23.34h

D. Experimental Details for Force Matching

D.1. Architecture

Müller-Brown Potential. For the MB potential, we use a radial basis function (RBF) feature map followed by a multilayer perceptron. The RBF expansion has $K = 100$ centers, initialized uniformly in $[10, 50]^2$ and optimized during training, with a fixed width $\sigma = 5.0$. The features are passed through four fully connected layers of size 128 with softplus activation, followed by a linear output layer.

Alanine Peptides. For peptides, the CG potential $U_\eta(\mathbf{R})$ is parameterized using the MACE architecture (Batatia et al., 2022), an equivariant message-passing graph neural network. Each CG bead is represented as a node in a geometric graph, with edges connecting neighbors within a cutoff radius and encoding relative position vectors. The model uses hidden irreducible representations of $32 \times 0e + 32 \times 1o$, processed through two interaction layers with correlation order 3 and an angular momentum expansion truncated at $\ell_{\max} = 3$. Node features are decoded by a readout layer ($16 \times 0e$) into a scalar energy prediction ($1 \times 0e$). Periodic displacement functions are applied during graph construction to handle boundary conditions correctly.

D.2. Training Configuration

For MB, training uses the Adam optimizer (via Optax) with a constant learning rate of 10^{-4} and batch size 128 for 500 epochs. For peptides, training uses Adam with exponential learning rate decay ($\eta_0 = 10^{-3}$, decay rate 0.01), batch size 256, and 300 epochs. We use 500k training samples for alanine dipeptide and 1000k training samples for alanine tripeptide and hexapeptide across all CG mappings. Training and validation splits are with a 90/10 ratio. Gradients are clipped to a global norm of 1.0. Validation losses in CG force matching are often noisy and do not consistently correlate with potential quality. We use the final training checkpoint for inference in all experiments.

D.3. Computational Cost

The reported inference times (Tab. 6) correspond to evaluating 10^4 samples. Training parameters follow §D.2. A batch size of 500 is used for inference.

Table 6. Training and inference time for MACE model on alanine dipeptide. Inference times correspond to 10^4 samples evaluated.

	Core Beta	Heavy Atom
Training	1.88h	4.11h
Inference	0.66s	0.72s

E. Compute Infrastructure and Software

E.1. Hardware

All experiments, including model training, inference, and computational benchmarks, are performed on a single NVIDIA A100 GPU with 80 GB memory.

E.2. Software

CFM is implemented using JAX, Difffrax (Kidger, 2021), and Flax (Heek et al., 2024). Graph transformer is adapted from the implementation provided in https://github.com/noegroup/ScoreMD/blob/main/src/scoremd/models/graph_transformer.py. Training of CG PMF is carried out using chemtrain (Fuchs et al., 2025b) and chemtrain-deploy (Fuchs et al., 2025a) built on JAX, M.D. (Schoenholz & Cubuk, 2020). Molecular structures are visualized using OVITO (Stukowski, 2009).

F. Algorithms

Algorithm 1 Training CG PMF via ESFM

Input: Dataset $\mathcal{D}_{\text{bias}} = \{(\mathbf{r}, \mathcal{F}_{\text{proj}}(\mathbf{r}))\}$ (Rapidly converged); batch size B
Initialize: CG PMF network U_η
while not converged **do**
 Sample $\{(\mathbf{r}^{(i)}, \mathcal{F}_{\text{proj}}^{(i)})\}_{i=1}^B \sim \mathcal{D}_{\text{bias}}$
 Compute $\mathbf{R}^{(i)} \leftarrow \Xi(\mathbf{r}^{(i)})$
 $\mathcal{L}_{\text{ESFM}} \leftarrow \frac{1}{B} \sum_{i=1}^B \|\nabla_{\mathbf{R}} U_\eta(\mathbf{R}^{(i)}) - \mathcal{F}_{\text{proj}}^{(i)}\|_2^2$
 Update $\eta \leftarrow \text{Optim}(\eta, \nabla_{\eta} \mathcal{L}_{\text{ESFM}})$
end while
Return U_η

Algorithm 2 Training Flow Model via CFM

Input: Dataset $\mathcal{D} = \{\mathbf{r}\}$ (biased or unbiased); batch size B
Initialize: flow model v_θ
while not converged **do**
 Sample $\mathbf{r}^{(i)} \sim \mathcal{D}$
 Compute $\mathbf{R}_1^{(i)} \leftarrow \Xi(\mathbf{r}^{(i)})$
 Sample $\mathbf{R}_0^{(i)} \sim \mathcal{N}(\mathbf{0}, \mathbf{I})$
 Sample $t^{(i)} \sim \mathcal{U}[0, 1]$
 $\mathbf{R}_t^{(i)} \leftarrow (1 - t^{(i)})\mathbf{R}_0^{(i)} + t^{(i)}\mathbf{R}_1^{(i)}$
 $u_t^{(i)} \leftarrow \mathbf{R}_1^{(i)} - \mathbf{R}_0^{(i)}$
 $\mathcal{L}_{\text{CFM}} \leftarrow \frac{1}{B} \sum_{i=1}^B \|v_\theta(t^{(i)}, \mathbf{R}_t^{(i)}) - u_t^{(i)}\|_2^2$
 Update $\theta \leftarrow \text{Optim}(\theta, \nabla_{\theta} \mathcal{L}_{\text{CFM}})$
end while
Return v_θ

Algorithm 3 Sampling & Reweighting

Input: Trained models U_η, v_θ ; number of samples N
 Initialize sample set $\mathcal{X} \leftarrow \emptyset$, log-weights $\mathcal{W} \leftarrow \emptyset$
for $i = 1$ to N **do**
 Sample $\mathbf{z} \sim \mathcal{N}(\mathbf{0}, \mathbf{I})$
 Solve ODE $\frac{d\mathbf{R}}{dt} = v_\theta(t, \mathbf{R})$ with $\mathbf{R}(0) = \mathbf{z}$
 $\mathbf{R}^{(i)} \leftarrow \mathbf{R}(1)$
 $\Delta \ell^{(i)} \leftarrow \int_0^1 \nabla \cdot v_\theta(t, \mathbf{R}(t)) dt$
 $\log q_\theta(\mathbf{R}^{(i)}) \leftarrow \log p_0(\mathbf{z}) - \Delta \ell^{(i)}$
 $E^{(i)} \leftarrow U_\eta(\mathbf{R}^{(i)})$
 $\log \tilde{w}^{(i)} \leftarrow -\beta E^{(i)} - \log q_\theta(\mathbf{R}^{(i)})$
 Append $\mathbf{R}^{(i)}$ to \mathcal{X} and $\log \tilde{w}^{(i)}$ to \mathcal{W}
end for
 Weight clipping for \mathcal{W}
 Normalize weights $\{w^{(i)}\}$ and compute ESS
Return samples \mathcal{X} , weights $\{w^{(i)}\}$, ESS

G. Additional Results

G.1. Müller-Brown Potential

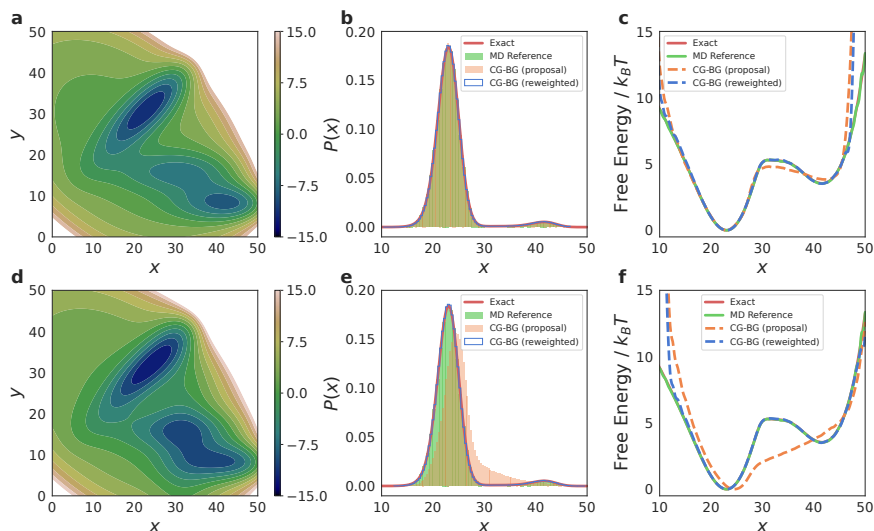


Figure 6. **CG-BGs on the MB potential.** (a) Two-dimensional unbiased MB potential energy surface (functional form in §B). (b) Marginal probability density along the x coordinate. (c) Free energy profiles before and after reweighting for CG-BGs, where flow is trained on *unbiased* data, compared with the exact solution and MD reference. (d-f) Same as (a-c), but for flow trained on *biased* data.

G.2. Alanine Tripeptide (Core Beta mapping)

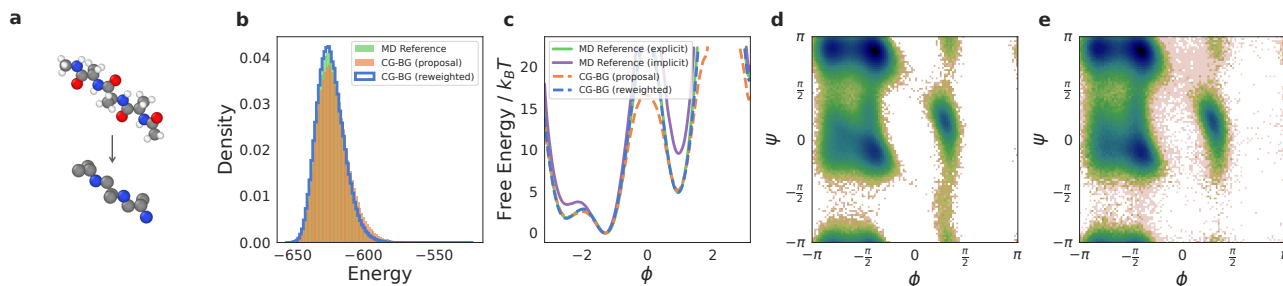


Figure 7. **CG-BGs on alanine tripeptide (Core Beta).** (a) Core Beta mapping. (b) Potential energy distribution under the learned PMF. (c) ϕ dihedral free energy profile. (d) MD reference Ramachandran plot. (e) Reweighted Ramachandran distribution obtained from CG-BGs.

G.3. Ramachandran Plots

We show Ramachandran plots for peptides to illustrate the effect of importance reweighting (Fig. 8 and Fig. 9), using MD reference distributions from explicit and implicit solvent simulations. The raw flow proposals exhibit noisy sampling and place probability mass in low-probability regions of the free energy landscape. These configurations receive low importance weights and therefore contribute negligibly after reweighting, yielding distributions that closely match the explicit solvent reference MD ensembles.

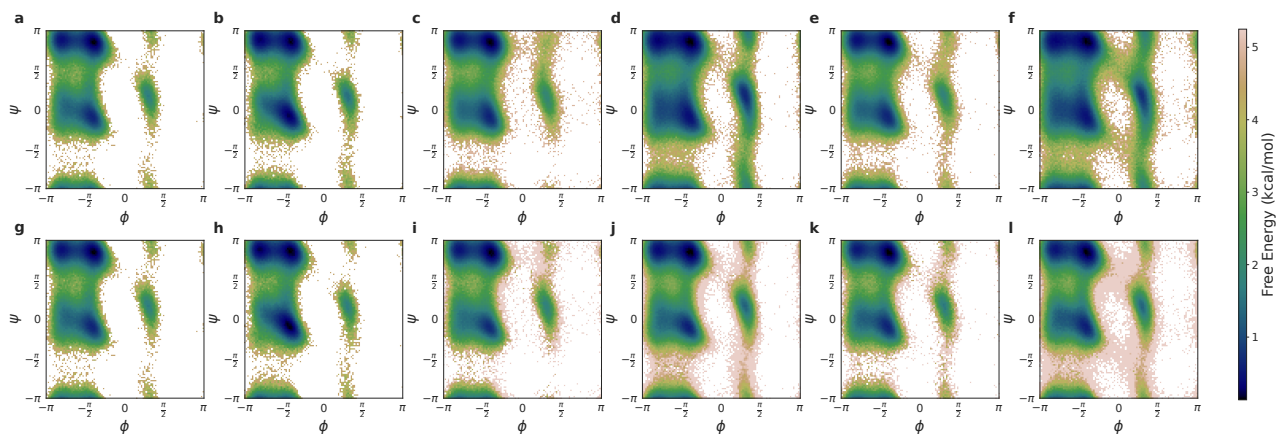


Figure 8. Ramachandran plots for alanine dipeptide. (a,g) Reference MD (explicit solvent). (b) Implicit solvent MD (OBC1). (h) Implicit solvent MD (OBC2). (c) Core Beta (unbiased) proposal. (d) Core Beta (WT-MetaD) proposal. (e) Heavy Atom (unbiased) proposal. (f) Heavy Atom (WT-MetaD) proposal. (i–l) Reweighted distributions corresponding to (c–f).

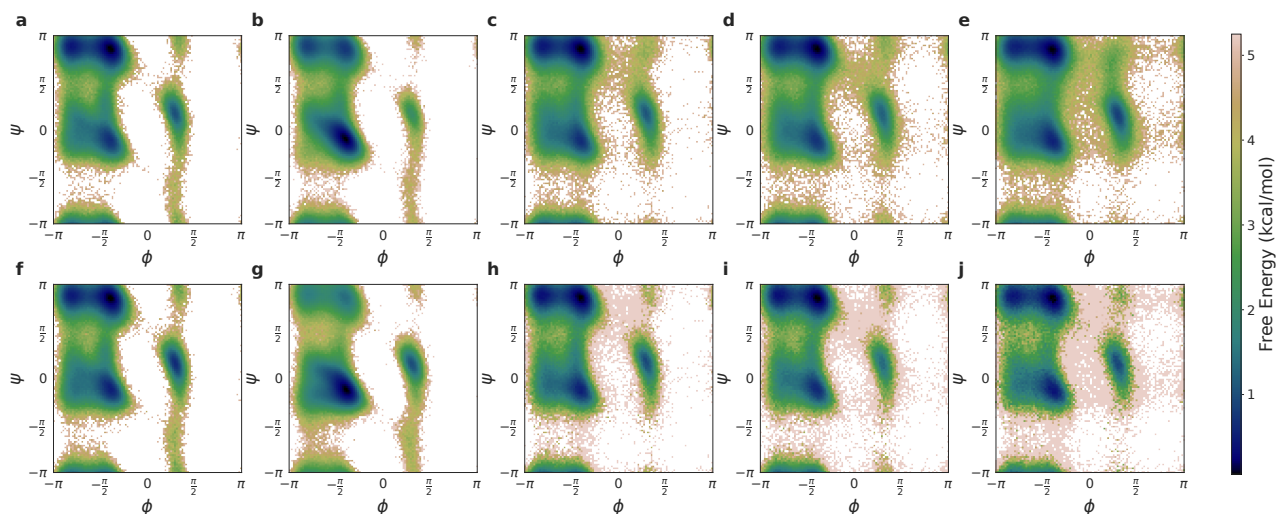


Figure 9. Ramachandran plots for alanine tripeptides and hexapeptides. (a,b) Reference MD for tripeptide (explicit and implicit solvent). (c,d) Flow proposals for tripeptide (Core Beta and Heavy Atom). (e) Flow proposal for hexapeptide (Core Beta). (f,g) Reference MD for hexapeptide (explicit and implicit solvent). (h–j) Reweighted distributions corresponding to (c–e).

G.4. Ablation of Weight Clipping

To stabilize importance reweighting, we apply a weight clipping strategy, discarding the top 1% of samples with the largest log-weights.

As shown in Tab. 7, Tab. 8 and Tab. 9, reweighting without clipping leads to large JS divergences and PMF errors, together with ESS, indicating severe weight degeneracy. In contrast, weight clipping restores stable estimates and substantially improves all metrics.

We further analyze sensitivity to the clipping ratio in Fig. 10. Aggressive clipping (10–20%) maximizes ESS but introduces bias in the reweighted distributions. Small clipping ratios (close to 0%) preserve unbiasedness but suffer from high weights variance. Balancing this bias–variance trade-off, we choose a conservative 1% clipping threshold across all experiments, which yields stable metrics while maintaining physically consistent distributions.

Coarse-Grained Boltzmann Generators

Table 7. Quantitative comparison for alanine dipeptide across CG resolutions and different weight clipping thresholds. Atomistic BG results from previous studies (Tan et al., 2025a) are included for reference, where models are trained on implicit solvent datasets and evaluated after reweighting using the implicit solvent energy function. Reported values are computed against the explicit solvent MD reference. For alanine dipeptide, TarFlow is trained on biased simulation data, which leads to low ESS.

Model	JS (\downarrow)	PMF (\downarrow)	ESS (\uparrow)
Flow Trained on <i>Unbiased</i> Dataset			
Heavy Atom Proposal	0.0048(1)	0.2749(72)	—
Heavy Atom Reweighted Proposal (1% clip)	0.0048(1)	0.2005(63)	0.5112(4)
Heavy Atom Reweighted Proposal (0% clip)	0.0065(1)	0.2548(91)	0.4038(28)
Core Beta Proposal	0.0058(1)	0.3662(85)	—
Core Beta Reweighted Proposal (1% clip)	0.0052(1)	0.2210(65)	0.5528(4)
Core Beta Reweighted Proposal (0% clip)	0.0065(1)	0.2833(84)	0.4592(50)
Flow Trained on <i>WT-MetaD</i> Dataset			
Heavy Atom Proposal	0.0510(3)	2.5527(382)	—
Heavy Atom Reweighted Proposal (1% clip)	0.0063(1)	0.2277(66)	0.4115(4)
Heavy Atom Reweighted Proposal (0% clip)	0.0058(1)	0.2163(61)	0.3603(23)
Core Beta Proposal	0.0437(2)	1.7185(294)	—
Core Beta Reweighted Proposal (1% clip)	0.0057(1)	0.2093(58)	0.4818(4)
Core Beta Reweighted Proposal (0% clip)	0.0058(1)	0.2015(55)	0.3939(11)
Atomistic BGs Trained on <i>Implicit Solvent</i> Dataset			
TarFlow	0.0548(2)	1.2696(314)	0.0034(18)
ECNF++	0.1451(19)	21.4005(4594)	0.2445(156)

Table 8. Quantitative comparison for alanine tripeptide across CG resolutions and different weight clipping thresholds.

Model	JS (\downarrow)	PMF (\downarrow)	ESS (\uparrow)
Flow Trained on <i>Unbiased</i> Dataset			
Heavy Atom Proposal	0.0065(1)	0.4071(73)	—
Heavy Atom Reweighted Proposal (1% clip)	0.0056(1)	0.1957(52)	0.3201(4)
Heavy Atom Reweighted Proposal (0% clip)	0.0110(1)	0.2926(184)	0.0368(192)
Core Beta Proposal	0.0061(1)	0.3800(71)	—
Core Beta Reweighted Proposal (1% clip)	0.0060(1)	0.2112(51)	0.4212(5)
Core Beta Reweighted Proposal (0% clip)	0.0414(2)	0.8451(142)	0.0018(10)

Table 9. Quantitative comparison for alanine hexapeptide across different weight clipping thresholds.

Model	JS (\downarrow)	PMF (\downarrow)	ESS (\uparrow)
Flow Trained on <i>Unbiased</i> Dataset			
Core Beta Proposal	0.0134(1)	0.9801(130)	—
Core Beta Reweighted Proposal (1% clip)	0.0100(1)	0.3646(81)	0.1231(3)
Core Beta Reweighted Proposal (0% clip)	0.1972(3)	8.0359(879)	0.0002(3)

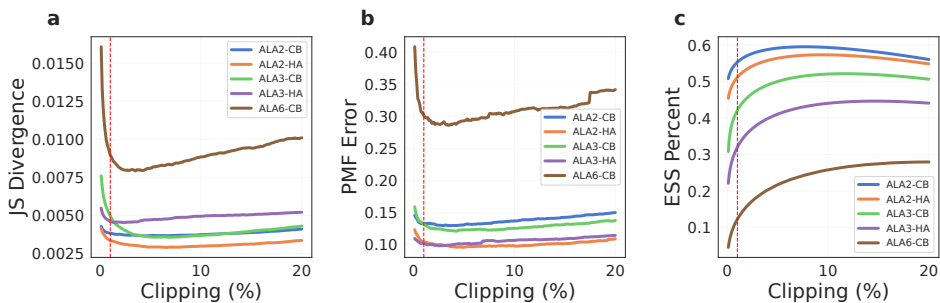


Figure 10. Metrics as a function of weight clipping ratio for flow models trained on unbiased datasets across different CG mappings and systems. (a) JS divergence, (b) PMF error, and (c) ESS after reweighting. The red dashed line indicates the 1% clipping ratio used throughout our experiments.

G.5. Free Energy of ψ Dihedral

We provide additional free energy plots for the ψ dihedral of alanine dipeptide (Fig. 11).

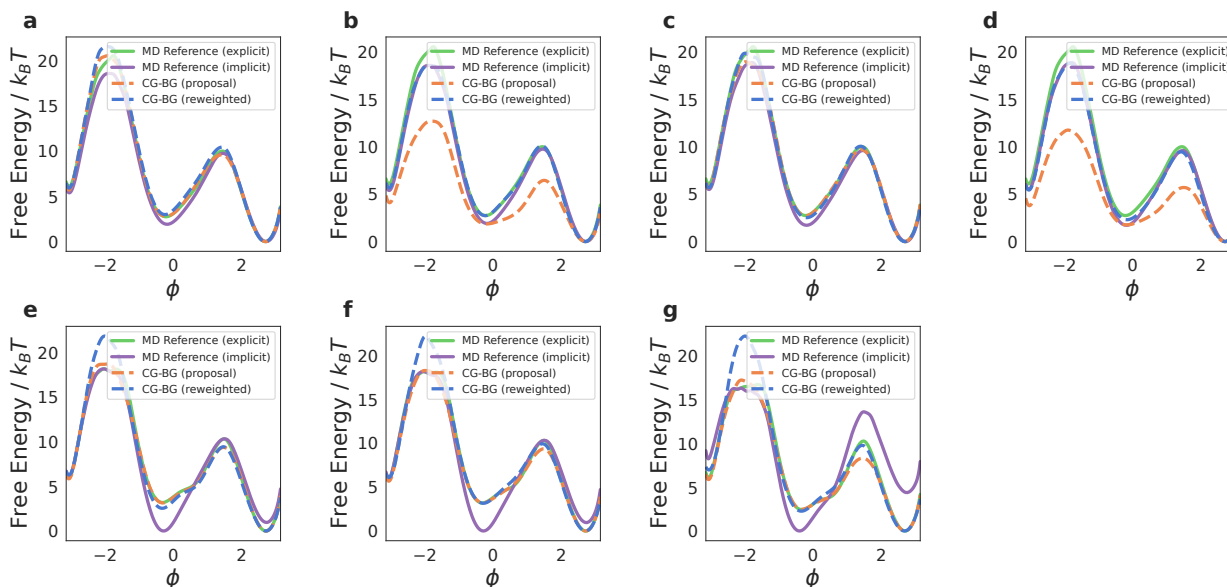


Figure 11. Comparison of ψ dihedral free energy profiles across training settings. All panels show MD reference distributions and CG-BG proposals before and after reweighting. (a) Dipeptide Core Beta (unbiased), (b) Dipeptide Core Beta (WT-MetaD), (c) Dipeptide Heavy Atom (unbiased), (d) Dipeptide Heavy Atom (WT-MetaD), (e) Tripeptide Core Beta, (f) Tripeptide Heavy Atom, (g) Hexapeptide Core Beta.

G.6. Bond Length

Fig. 12 shows the C–N bond length distributions for the MD reference and CG-BG results before and after reweighting.

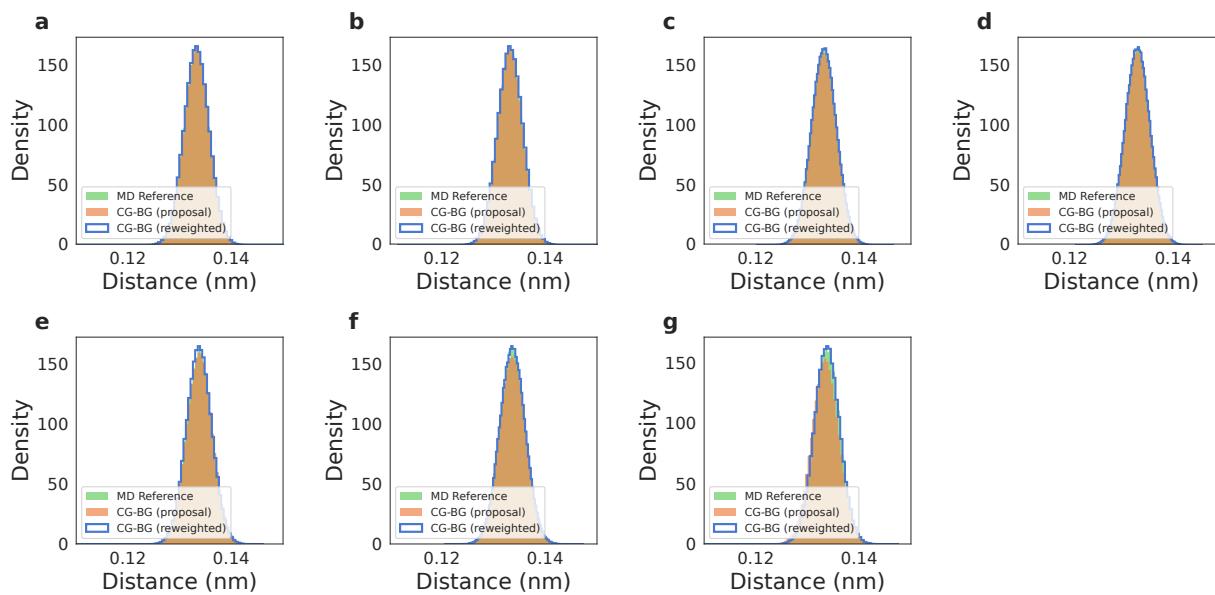


Figure 12. Comparison of C-N bond length distributions across training settings. All panels show MD reference distributions and CG-BG proposals before and after reweighting. (a) Dipeptide Core Beta (unbiased), (b) Dipeptide Core Beta (WT-MetaD), (c) Dipeptide Heavy Atom (unbiased), (d) Dipeptide Heavy Atom (WT-MetaD), (e) Tripeptide Core Beta, (f) Tripeptide Heavy Atom, (g) Hexapeptide Core Beta.